Master's Thesis

Platform for Low-Power Driving Wireless Pressure Sensor with Instant Visualization

Woon Hyung Cheong

Department of Materials Science and Engineering

Graduate School of UNIST

2019

Platform for Low-Power Driving Wireless Pressure Sensor with Instant Visualization

Woon Hyung Cheong

Department of Materials Science and Engineering

Graduate School of UNIST

Platform for Low-Power Driving Wireless Pressure Sensor with Instant Visualization

A thesis/dissertation
submitted to the Graduate School of UNIST
in partial fulfillment of the
requirements for the degree of
Master of Science

Woon Hyung Cheong

06/10/2017 of submission
Approved by

_____

Advisor
Myoung Hoon Song

Platform for Low-Power Driving Wireless Pressure Sensor with Instant Visualization

Woon Hyung Cheong

This certifies that the thesis/dissertation of Sung-Ho Shin is approved.
2019 of submission

Signature

_____

Advisor : Myoung Hoon Song

Signature

_____

Jang-Ung Park

Signature

_____

Sang-Young Lee

`

Abstract

Wireless communication through linkage with a smartphone and other portable devices in the sensor area is essential from the viewpoint of increasing the efficiency of utilization through storing data of the sensing value. On this account, the wireless technology is of increasing in demand due to advantages they have for various applications using this data. However, there is still considerable ambiguity for the low portability due to the large volume in the implementation area of the system for wireless communication in the pressure sensor, the high-power consumption and the necessity of separate battery. Herein, we solve this problem through miniaturization of the device through the structure of built-in battery, low power driving technology using a pressure-active switch, and implementation of wireless communication platform through the integration of Bluetooth module and devices. Furthermore, the wireless transmission of the pressure-sensing results is demonstrated in this paper. In addition, we implemented and demonstrated a human-interactive display that enables users to visualize instantly through brightness change of organic light-emitting diodes (OLED) according to pressure. We show the system of displaying the pressure value measured in real time on the screen of the mobile devices which is expected to advance in the fields of soft electronics and biomedical science. In order to improve the portability of the pressure sensor and improve the applicability, the process was performed on a new substrate through hybridization of the rigid part and the soft part so as to allow conformal contact to curved objects as well as rigid glass-based substrates. Through the process in the rigid part, the protection of the main components is ensured and flexibility and stretchability are ensured by the deformation of the soft part. Because it is applicable to various biocomponents such as organ organs, insects or surface of plants, the pressure sensor using this structure has wide expandability in biomedical field.

Contents

Abstract ····· i
Contents ····· ii
List of Figures ····· v
1. Introduction ····· 1
1.1 Research background and motivation ····· 1
1.2 Research objectives and contents ····· 7

2. Pressure sensor with Low-Power driving ····· 8
2.1 Research background ····· 8
2.2 Experiments ····· 11
2.2.1 Experimental Methods ····· 11
2.2.2 Results and discussion ····· 13
2.2.3 Conclusion ····· 29

3. Integrated wireless system with pressure sensor ····· 30
3.1 Research background ····· 30
3.2 Experiments ····· 31
3.2.1 Experimental Methods ····· 31
3.2.2 Results and discussion ····· 33
3.2.3 Conclusion ····· 38

4. Conclusion ····· 39
5. References ····· 40
6. Acknowledgements ····· 44

`

List of Figures

Figure 1.1 Growth of IoT market and Human-machine interface devices.

Figure 1.2 Applying wireless communication system to the conventional devices

Figure 1.3 Medical devices with wires / recently reported wireless sensors

Figure 1.4 Conventional pressure sensor with various application and biomarker for health information

Figure 1.5 Problem statement for current issues with solution

Figure 1.6. Research contents

Figure 2.1. Previous attempt for making outstanding performance of pressure sensor

Figure 2.2. Theoretical background for air-dielectric field effect transistor

Figure 2.3. Integrated system for wireless transmission of sensed pressure with pressure sensor

Figure 2.4. Experimental method of FET based pressure sensor with air-dielectric

Figure 2.5. Schematic of the integrated system, consisting of the pressure sensor, built-in battery, and wireless Bluetooth module.

Figure 2.6. Transfer characteristics of the single pressure sensor with V_D = 10 V.

Figure 2.7. Optical microscope image of each component of the pressure sensor array and a zoom-in image of a pixel of pressure sensor showing the pressure-sensitive switch, isolated Si channel, and OLED. Scale bar, 300 μm.

Figure 2.8. Photographs of the built-in battery which is directly manufactured on the back of the pressure sensor.

Figure 2.9. Electrical current change due to applied pressure (60 kPa).

Figure 2.10. (a) The response time (~110 ms) and (b) recovery time (~120 ms) of the single pressure sensor which is measured by in real-time current plot.

Figure 2.11. Contact resistance of the switch. The resistance is measured at VD = 5 V and constant pressure at 6 kPa with pressure application device (mark-10), the measurement was carried out 100 times under the same conditions. The contact resistance is under 35 ~ 40 Ω, which is negligible to affect the pressure sensor.

Figure 2.12. Transfer characteristics (I_D-V_G curve, V_D = 2V ~ 18 V in 2 V step) of the FET through the OLED

Figure 2.13. Schematic of the operating mechanisms of the switch and the pressure sensor when external pressure is applied.

Figure 2.14. Transfer characteristics (I_D-V_G curve, V_D = 5 V) of the pressure sensor with the exception of the switch for the variation of applied pressure (0 kPa ~ 700 kPa).

Figure 2.15. Output current change of the device with the variation of applied pressure in real time (V_D = 5 V, V_G = 10 V). Each step can be separated over a range of minimum pressures to operate the switch.
Figure 2.16. Pressure sensing apparatus. A motorized vertical test stand (Mark-10 ESM303) in combination with a force gauge (Mark-10 M7–20).
Figure 2.17. Intensity change of the light emitted from OLED connected in series with the variation of applied pressure.
Figure 2.18. Comparison between luminescence responses of the fabricated device (pressure sensor - OLED) and true stress-strain curve from PDMS film compression test.
Figure 2.19. Comparison of response value for pressure sensor with presence or absence of switch under the same applied pressure of 60 kPa in real time.
Figure 2.20. Comparison of power consumption with presence or absence of switch when the repetitive pressure sensor operation is performed.
Figure 2.21. Cyclic test of the pressure sensor under the pressure of 60 kPa.

Figure 3.1. Integrated system with pressure sensor and Bluetooth module.
Figure 3.2. Actual photographs of communication module. (a) Structure of connection between MCU and Bluetooth module. Two boards are connected with board-to-board connector (elevated pin header). (b) Connection between sensor electrode pad and flat, flexible cable (FFC) by ACF bonding. (c) Connection between MCU and FFC with strap holder. (d) Connection between contact pad of Bluetooth module and interconnect of printed built-in battery by soldering technique.
Figure 3.3. Actual photographs of integrated module with the part of MCU and Bluetooth.
Figure 3.4. Corresponding electrical circuitry for active-matrix sensor array which allows selective readout of electrical response and wireless transmission to the smartphone.
Figure 3.5. Photographs of integrated device which is composed of pressure sensor, built-in battery, and Bluetooth module. Scale bar, 2 cm.
Figure 3.6. Photographs of single sensor pixel that emit light in response to applied pressure and captured images of a smartphone which received pressure information by wireless communication.
Figure 3.7. Photographs of sensor array that emit light in response to applied pressure and captured images of a smartphone which received pressure information by wireless communication.
Figure 3.8. Displayed pressure force imposed at the sensors on the screen of the smartphone through Bluetooth wireless communication

`

1. Introduction

1.1. Research background and motivation

As the development of Internet of things (IoT) [1,2] and human-machine interactive devices has expanded its role, it is required to have a high level of portability and a function in interoperating with a smartphone so that it can be used conveniently in daily life. By linking such a portable device with a smartphone, the result of the export from the device can be converted into data that can be displayed directly on the screen of either the computer or the smartphone. In the area of sensors, the increase in usability due to the conversion of these measurement results is directly related to the expansion of the application field [2–4]. Therefore, wireless communication has become an essential element in every field of electronics.

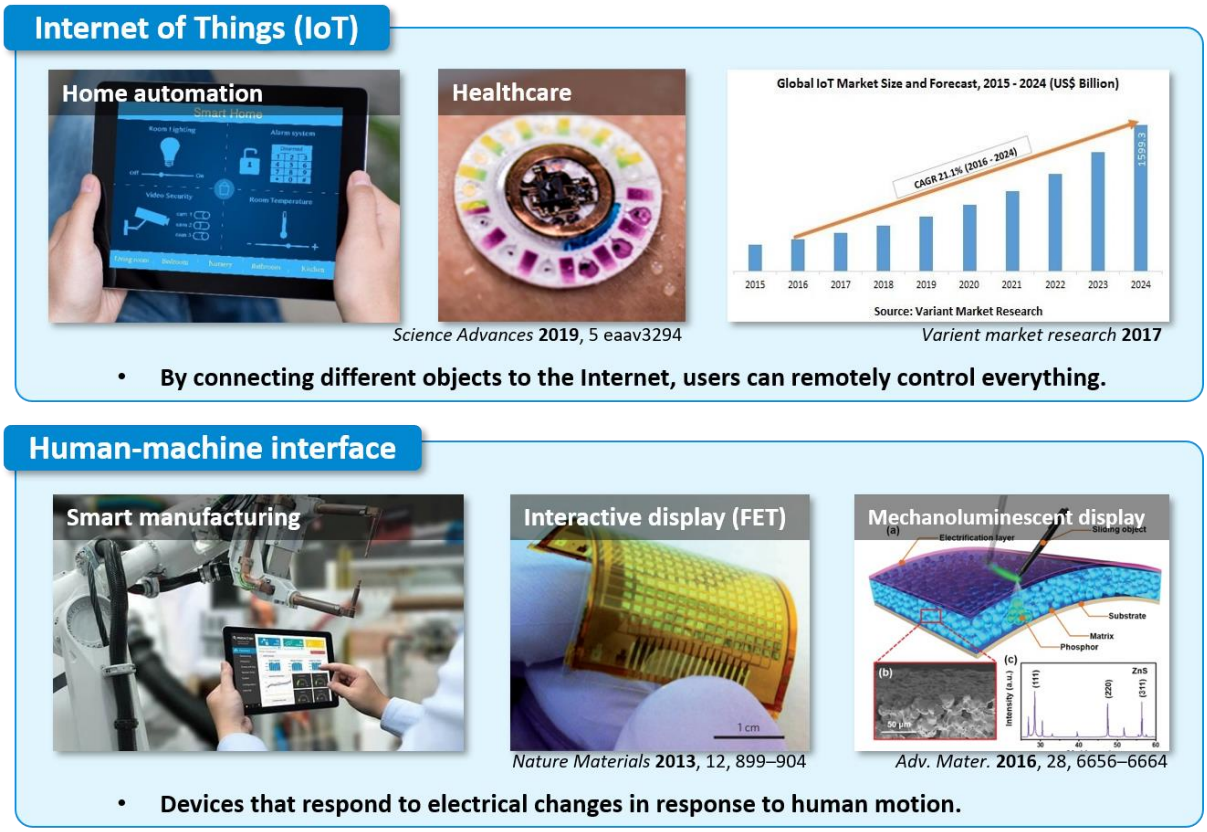

Figure 2.1 Growth of IoT market and Human-machine interface devices

`

Conventional devices are having crucial disadvantages in spatial problem that is not portable. These devices such as a pressure mapping sensor and a robot hand have so many wires that cannot move easily. But by connecting these devices by wireless communication system, devices can accumulate and utilize various data that can be obtained from sensing.

Figure 3.2 Applying wireless communication system to the conventional devices

Conventional medical devices have so many wires, so people have to stay in the hospital during their medical treatment. But by integrating with wireless system, these sensors can operate in people's normal daily life. Thus, the key point is applicability of sensors are expanded due to wireless communication, high portability improves user convenience, and it is possible to receive various information values from various places.

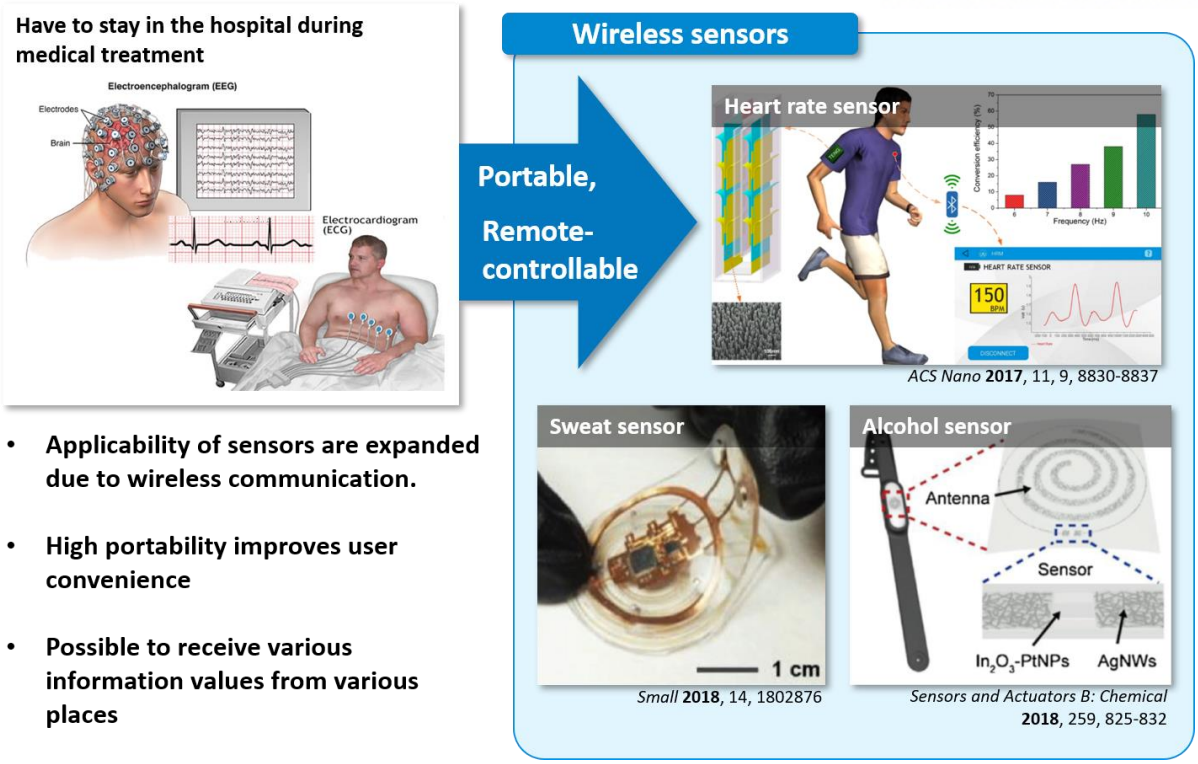

Figure 1.3 Medical devices with wires / recently reported wireless sensors

Conventional pressure sensors have various mechanical and electrical pressure sensing methods such as piezoelectric [5], piezoresistive [6], and capacitive sensing mechanisms [7,8]. Among the conventional sensors, field-effect transistor (FET) type pressure sensors are most widely used in electronic devices, which makes it easy to use them with other additional parts and can be achieved the least crosstalk from the use of the active-matrix structure. In addition, various studies using the structural characteristics of the FET type are underway [9].

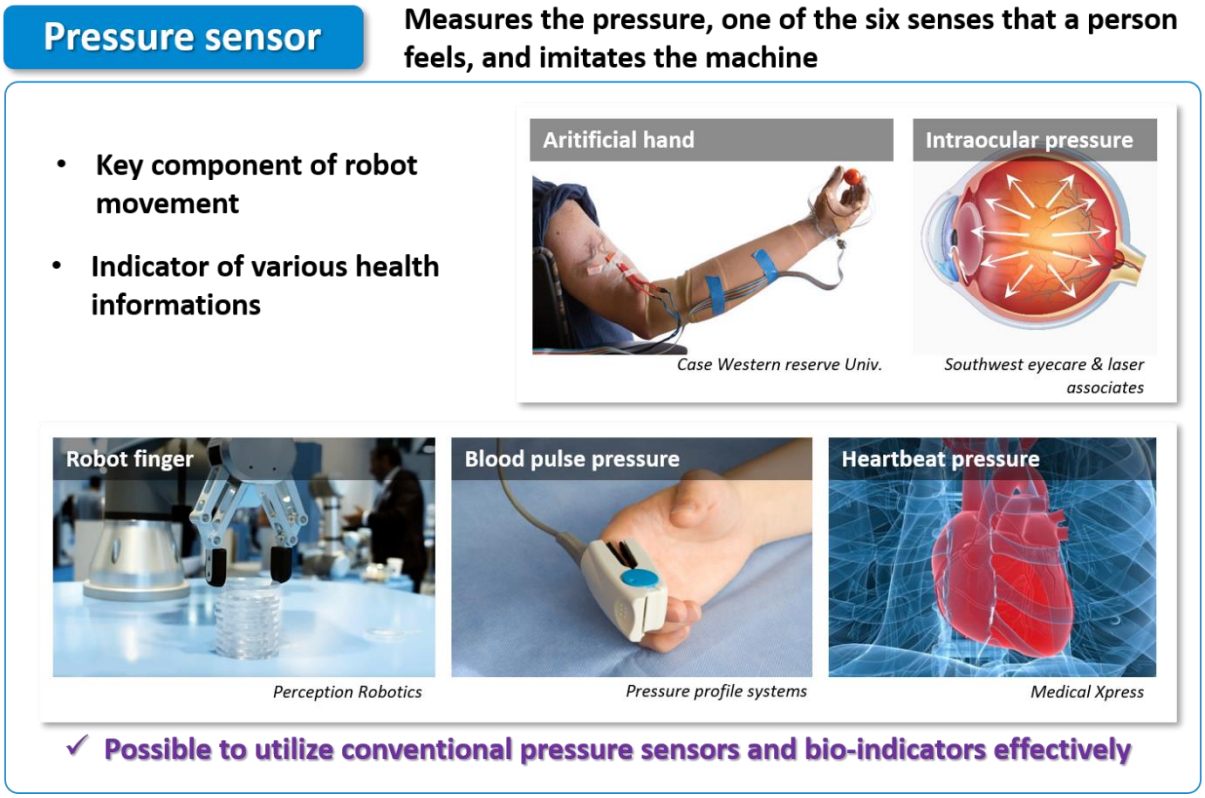

Figure 1.4 Conventional pressure sensor with various application and biomarker for health information

Among them, researches of measuring the pressure over a wide range by changing the thickness according to the external contact by replacing the dielectric layer with air have recently been announced [10,11]. However, despite these advantages, it requires bulky equipment for operating the entire system such as external power sources, measuring device for reading the electrical signal and therefore it has low portability. Also, even if the electrical signal of the sensor is transmitted, it is hard to apply it to other electric devices except for additional wire.

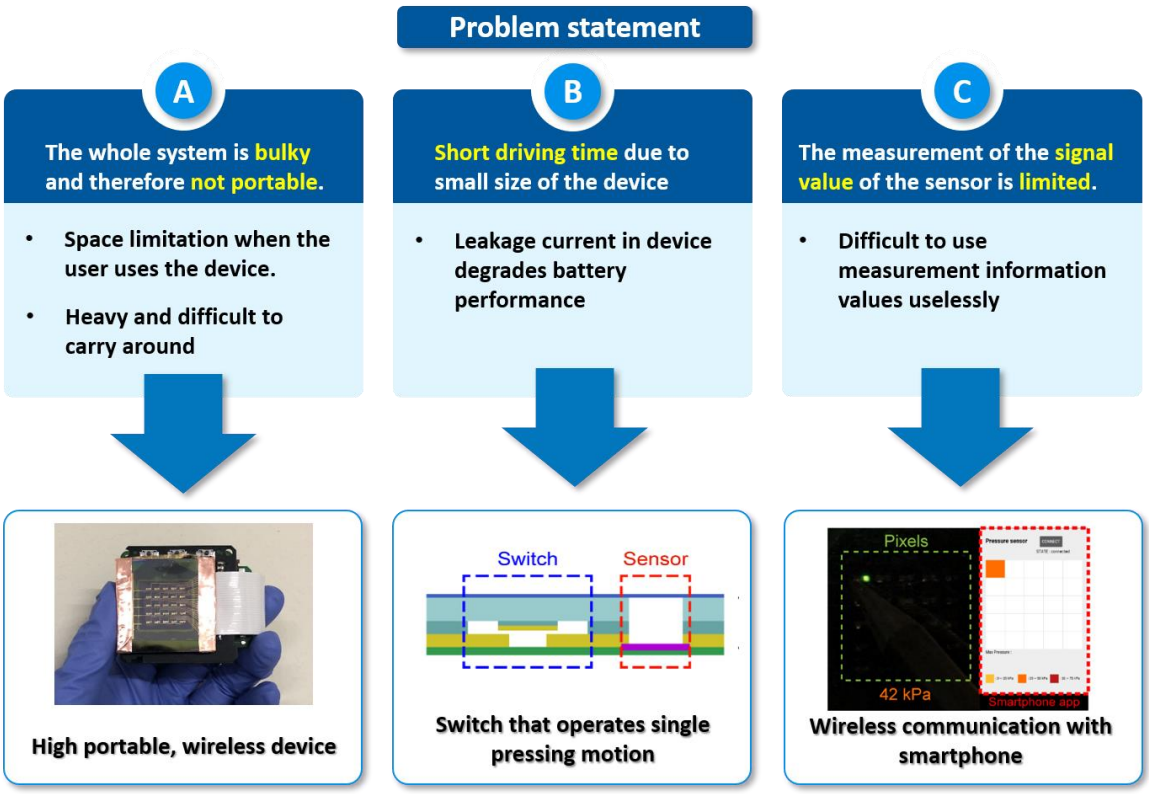

Figure 1.5 Problem statement for current issues with solution

Herein, we developed a system that can minimize the volume, weight, and driving voltage of devices by integrating a built-in type battery produced by a direct printing method on the backside of the sensor substrate [12,13], a pressure sensitive switch that enables low power drive by eliminating the standby power consumption [14], and a wireless communication module which enables remote interoperation with the external source [4,7,15].

`

The device transmits the data of pressure to either a smartphone or other receiving devices when the user presses the pixel consisting of the pressure sensor, and by connecting the Bluetooth module together, wireless communication with the smartphone records and stores information about the pressure, thereby enhancing the utilization of the data of the sensor. In this regard, we did demonstrations of converting pressure-sensing feedback into electrical signals with the device constructed of Bluetooth module [16], pressure sensor, and battery. Converted electrical signals were transmitted to the Bluetooth module and displayed on the screen of the smartphone immediately.

In the sensor array, OLEDs responsive to pressure are formed so that the user can visually receive the pressure information [15], and the OLED intensity visualized is dependent on both the size of the device and the amount of pressure. Through the construction of a system capable of these wireless communications, we expect the expansion of the field of the sensor by enabling free conversion of the results of the sensor to digital data. Accordingly, results have been very promising so far to advance in the field of soft electronics and biomedical science through the technologies that enable wireless communication system between electronic sensors and mobile devices, therefore miniaturization and low driving power of devices.

1.2. Research objectives and contents

The main objects for the research is to develop the wireless communication system with integration of the pressure sensor, switch for the low-power driving device, OLED for visualization of sensed pressure [13,17,18]. With the successful demonstration of the real device of integrated system, smartphone application for wireless communication system also be included. It is also aimed to confirm the possibility of device by various attempts such as shape change of substrate and material change in order to establish the foundation for applying it to other useful places after device operation. Following figure shows the schematic diagram for the research presented in this paper.

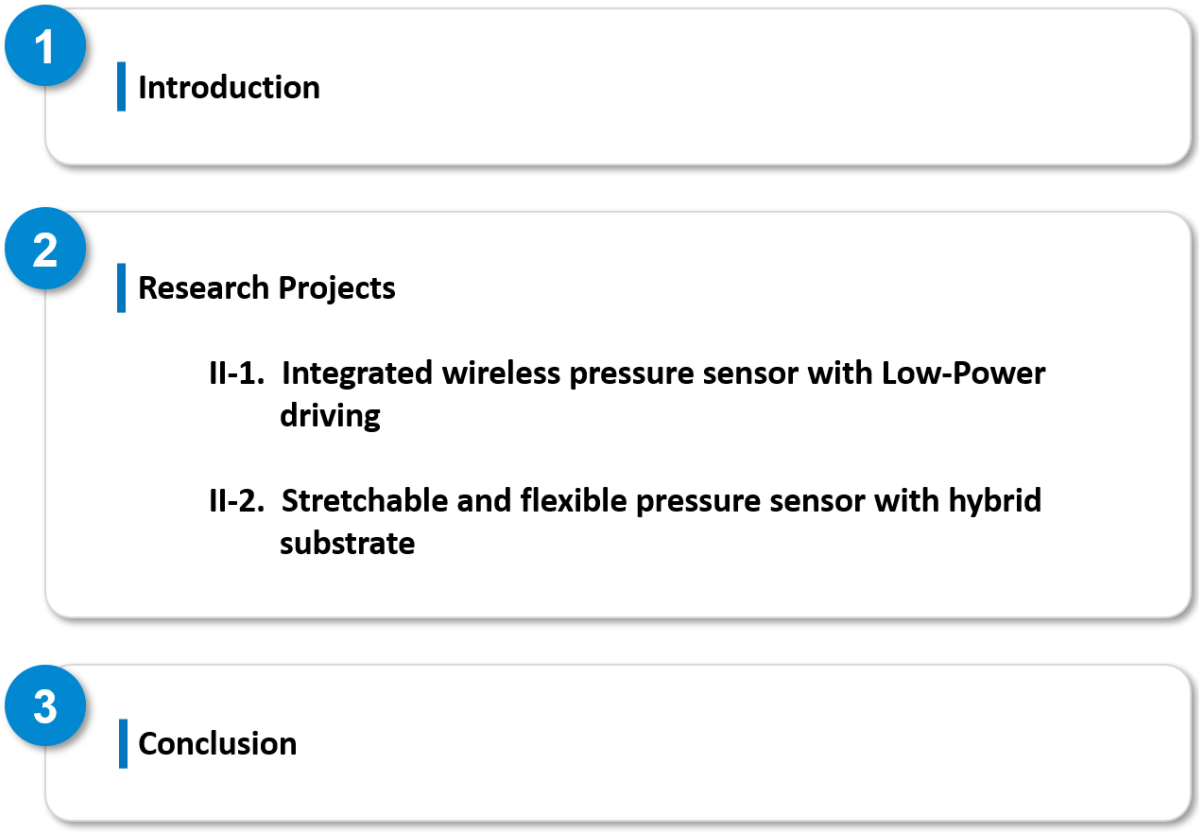

Figure 1.6. Research contents

`

2. Pressure sensor with Low-Power driving

2.1. Research background

In previous research, various attempts to make pressure sensors that have outstanding performance have been studied. In specially, field-effect transistor type pressure sensors have been studied widely, due to their active-matrix structure. However, they need to be integrated with additional pressure-sensing components such as conductive and pressure-sensitive elastomers [4].

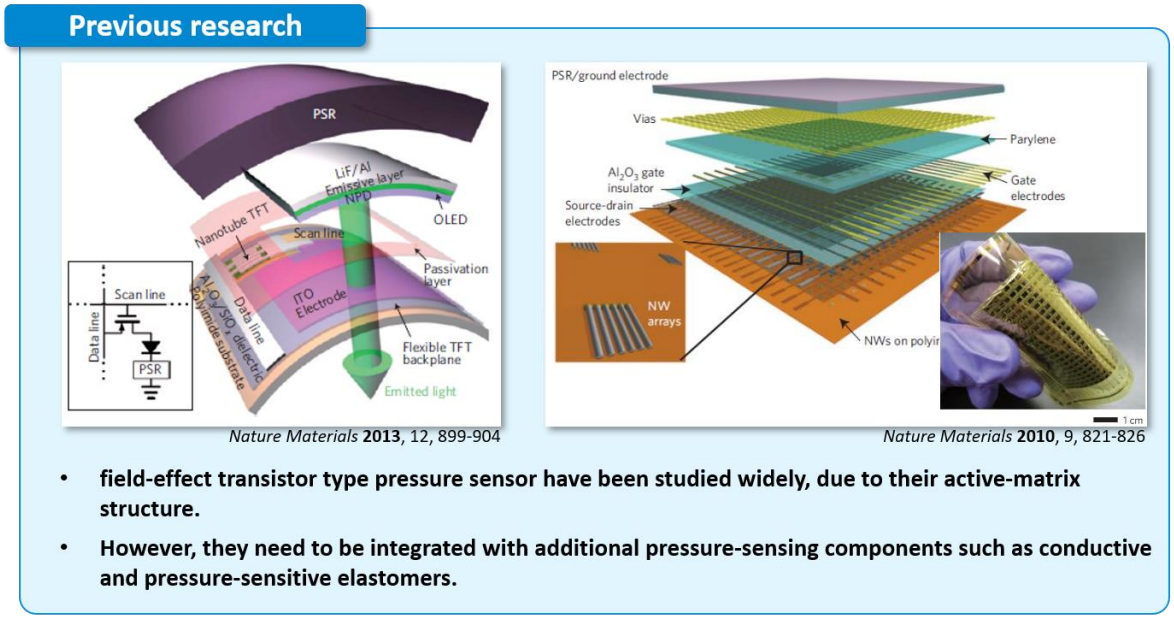

Figure 2.1. Previous attempt for making outstanding performance of pressure sensor

Therefore, to solve these disadvantages, the pressure sensor's dielectric layer is replaced to air, by fabricating the side wall with PDMS and SU8 photoresist, so that the gate electrode is located in upper the channel, in free-standing form [10].

Because of the elastic property of PDMS, when pressure is applied to sensor, variation in the thickness of the dielectric layer due to pressure changes the gating effect on the channel. It leads the change of capacitance, and therefore the threshold voltage is changed. This pressure sensitive transistor can be used as a pressure sensor without any other additional sensing component

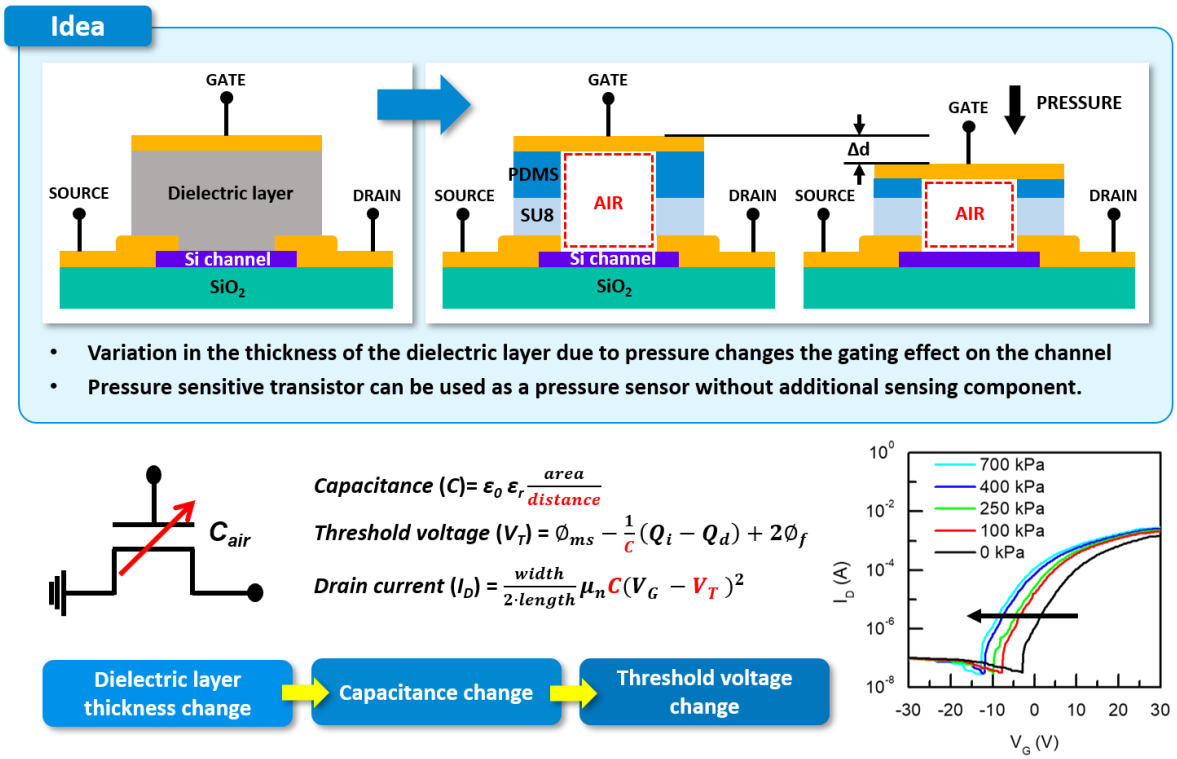

Figure 2.2. Theoretical background for air-dielectric field effect transistor

`

For making such device, OLED and switch is added next to the sensor so that a switch to provide electrical disconnection when no pressure is applied. This make pressure sensor to be more energy-efficiently.

Also, connecting OLED for visually expressing current change in pressure sensor is made for immediate feedback for human touching motion [12].

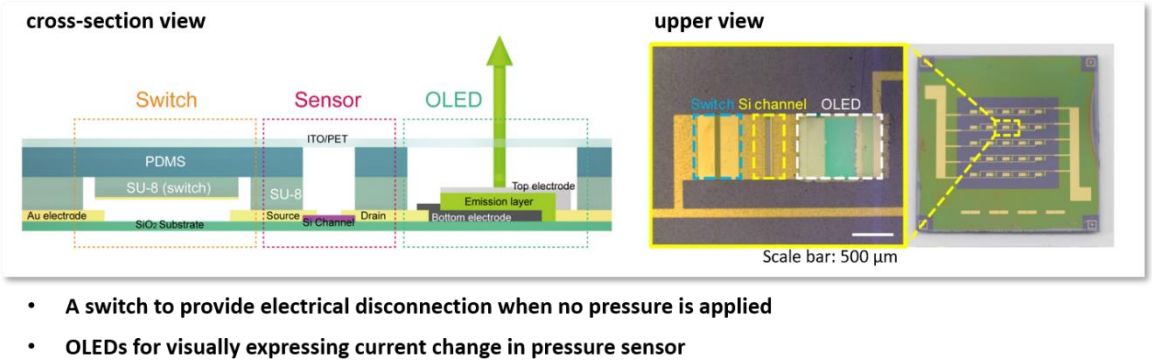

Figure 2.3. Integrated system for wireless transmission of sensed pressure with pressure sensor

`

2.2. Experiments

2.2.1. Experimental methods

[Preparation of the FET with air-dielectric and Si channel layer]

For fabrication of the Si channel layer, a patterned FET channel with a single-crystalline Si layer (width: 120 nm; length: 600 nm; thickness: 340 nm) was formed on a silicon-on-insulator (SOI) wafer (buried oxide 400 nm, Soitec) by photolithography and reactive ion etching. Cr/Au electrodes (thicknesses: 5 nm/100 nm) were deposited thermally and patterned to serve as the source and drain electrodes of the FET. Subsequently, a negative photoresist (SU-8, MicroChem) was patterned using photolithography to form a spacer so that an air gap (depth: 10.5 μm) could be used as the dielectric layer of FET. In order to change the thickness of the air gap in response to pressure, polydimethylsiloxane (PDMS) was coated on the indium tin oxide (ITO) layer on a polyethylene terephthalate (PET) film to form a gate electrode layer. We fabricated a layer of PDMS (thickness: 30 μm) on the ITO-PET film using spin coating, and we cured it slowly at a low temperature to keep the elastic modulus of the PDMS as low as possible. The ITO gate electrode was patterned by wet etching so that the selective gate electrode remained partially above the FET channel, and then a laser was used to cut the PDMS off of the channel portion to minimize the charge-accumulation effect due to the PDMS.

[Fabrication of top-side emissive green OLEDs]

For the integration of small-molecule OLED, we used sophisticated magnetic mask for patterning. As the first step, Al electrodes (thicknesses: 100 nm) were deposited into a vacuum chamber (HS-1100, Digital Optics & Vacuum) for continuous thermal evaporation of various organic and inorganic layers. Top-side emissive OLEDs had following structure: Al(100 nm)/MoO_3(10 nm)/TCTA(40 nm)/TCTA: $Ir(ppy)_3$ (8 wt%, 20 nm)/B3PyMPM (60 nm)/ LiF (1 nm)/Al (1 nm)/Ag (35 nm), where TCTA is tris (4-carbazoyl-9-ylphenyl)amine and $Ir(ppy)_3$ is Tris(2-phenylpyridinato-C2,N)iridium(III) which has low efficiency roll-off without complex process of co-doping(exiplex) system.

[Fabrication of built-in battery]

The unit cell, which has a voltage of 2.7 V, consists of the printed $Li_4Ti_5O_{12}$ (LTO) anode, the $LiCoO_2$ (LCO) cathode, and a solid-state electrolyte. The thermally-stable electrolyte was made of 1 M LiPF6 in ethylene carbonate (EC, boiling point = 261 ºC)/propylene carbonate (PC, 242 ºC) = 1/1 (v/v); an UV-cured, ethoxylated trimethylolpropane triacrylate (ETPTA) polymer matrix; and alumina (Al_2O_3) nanoparticles that act as a rheology-tuning agent. The cross-sectional scanning electron microscopy (SEM) image of the unit cell (right side of Fig. 3a) shows the seamless unitization of the printed LTO anode, the solid-state electrolyte, and the LCO cathode. Fig. 3b shows the ion/electron transport behavior in the unit cell and the structure and components of the printed electrodes and the solid-state electrolyte.

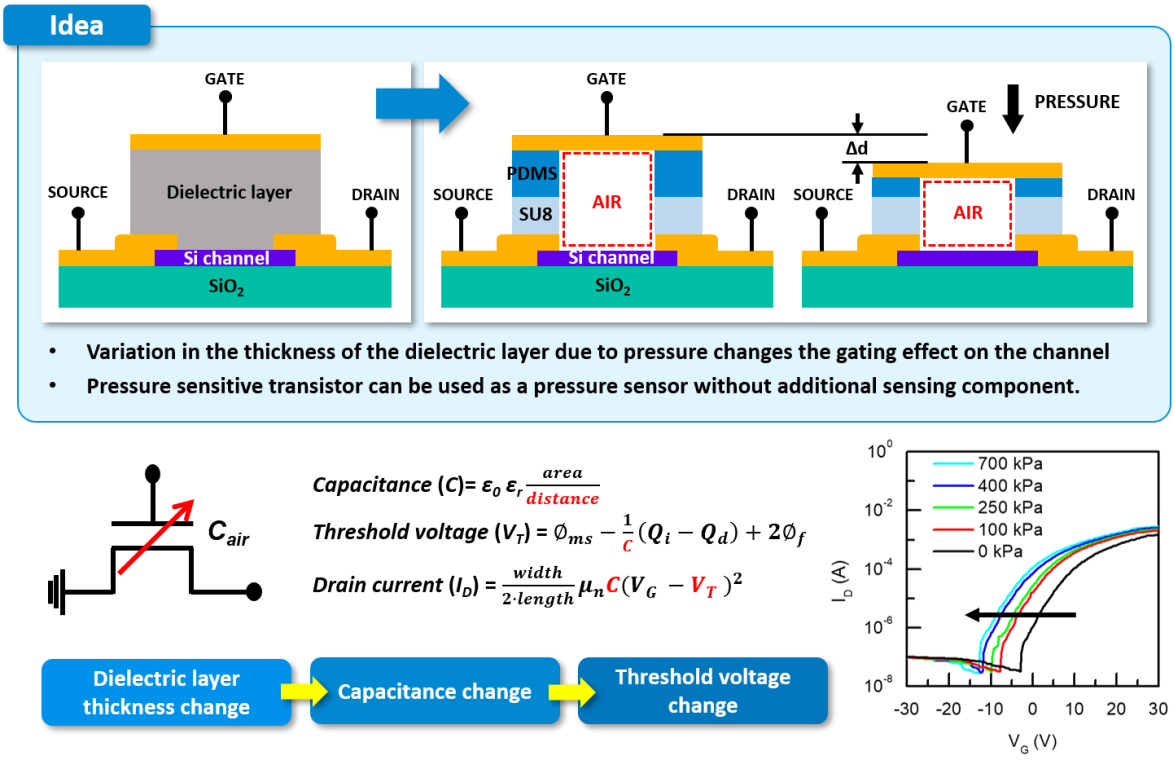

Figure 2.4. Experimental method of FET based pressure sensor with air-dielectric

`

2.2.2. Results and discussion

[Integrated system of pressure sensing]

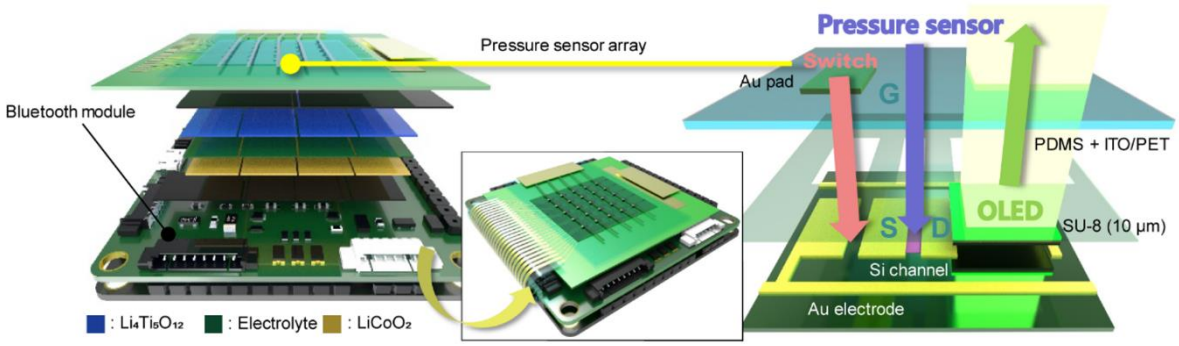

Figure 2.5. Schematic of the integrated system, consisting of the pressure sensor, built-in battery, and wireless Bluetooth module.

The left side of Figure 2.5 is an integrated schematic of a transistor-based pressure sensor, a printed-battery, and a module that enables wireless communication with a smartphone using Bluetooth. The pressure sensor and the battery were formed on the front and back sides of the Si substrate and were packaged together. The Bluetooth communication module and sensor are connected with a dedicated strap, which minimizes entire volume of integrated devices and provides the simple integration structure [19].

As shown on the right side of Figure 2.5, the pressure sensor is constructed from three components. Switches that control the flowing current level into the pressure sensor, a transistor-type pressure sensor, and an OLED that visualizes the change in current as the pressure increases are connected in series. For this fabrication, a patterned FET channel with single-crystalline Si layer (width: 120 nm, length: 600 nm, thickness: 340 nm) was formed on silicon-on-insulator (SOI) wafer (buried oxide 400 nm, Soitec) by photolithography and reactive ion etching. Cr / Au (thickness: 5 nm / 100 nm) electrodes are thermally deposited and patterned as roles of source and drain electrodes of FET. Subsequently, a negative photoresist (SU-8, MicroChem) was patterned using photolithography to form a spacer to use an air gap (depth: 10.5 μm) as the dielectric layer of FET.

`

Since it is necessary to partially expose the switch and the channel region for the sensor and OLED at the same time, we considered this simultaneously and patterned together by photolithography. In order to change the thickness of the air gap in response to pressure, Polydimethylsiloxane (PDMS) was coated on the Indium tin oxide (ITO) layer on a Polyethylene terephthalate (PET) film to form a gate electrode layer. We fabricated a layer of PDMS (thickness: 30 μm) on the ITO-PET film using spin coating and cured slowly at low temperature to keep the PDMS elastic modulus as low as possible. The ITO gate electrode was patterned by wet etching so that the selective gate electrode partially remained above the FET channel, and PDMS was then cut off the channel portion using laser cutting to minimize the charge accumulation effect due to PDMS.

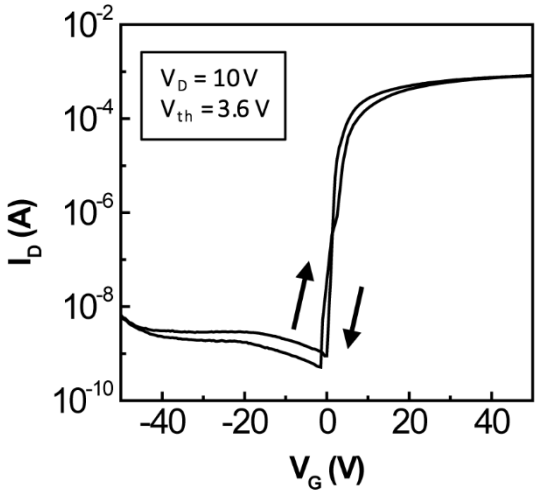

Figure 2.6. Transfer characteristics of the single pressure sensor with V_D = 10 V.

The transfer characteristics of the FET sensor are shown in Figure 2.6. SU-8 was patterned on the cured PDMS in the form of an island (width: 650 nm, length: 850 nm) by photolithography to produce a switch operating system activated as the pressure is being applied. Afterward, Cr / Cu / Au (3 nm / 500 nm / 50 nm) was thermally deposited on the SU-8 island through a shadow-masking technique to fabricate a conductive switch.

`

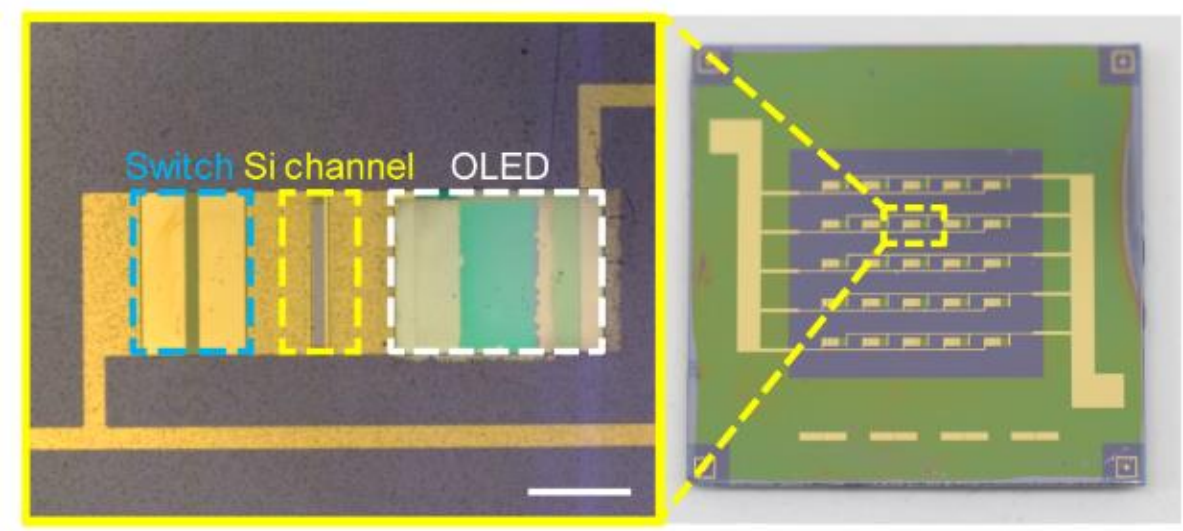

Figure 2.7. Optical microscope image of each component of the pressure sensor array and a zoom-in image of a pixel of pressure sensor showing the pressure-sensitive switch, isolated Si channel, and OLED. Scale bar, 300 μm.

Figure 2.7 is an optical microscope image of each component of the pressure sensor. The electrodes of the switch are intentionally open-circuited, so that when the conductive switch contacts both ends of open electrodes due to pressure, current flows toward the OLED arrays so that the pressure information can be converted to a visualized light source. The switch configuration is defined by the SU-8 spacer which forms an air gap to prevent electrical contact of both sides of electrodes when pressure is not applied.

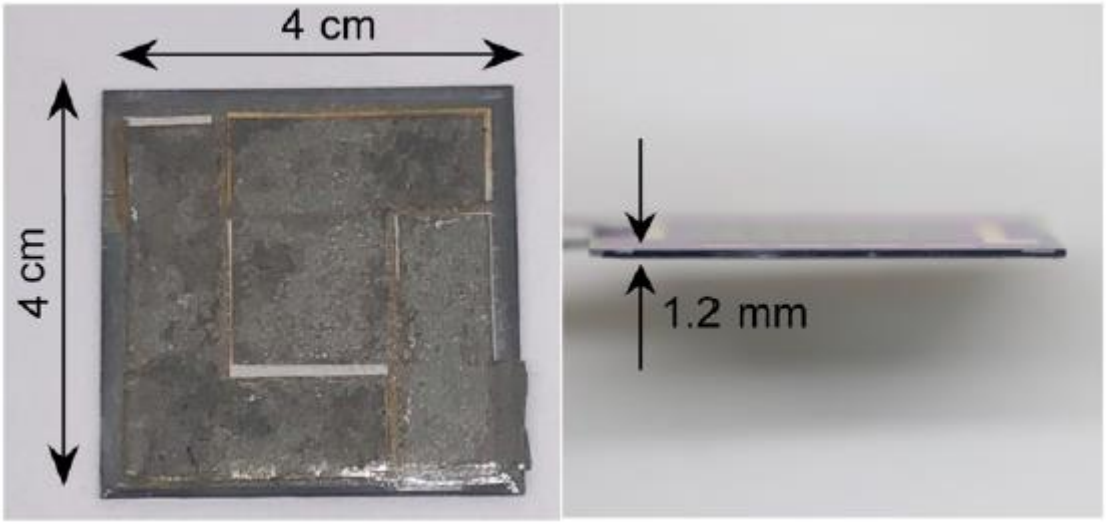

Figure 2.8. Photographs of the built-in battery which is directly manufactured on the back of the pressure sensor.

Figure 2.8 exhibits photographs of the built-in battery which is directly manufactured on the backside of the pressure sensor. The battery is small enough not to leave the pressure sensor substrate area (area of sensor substrate: 16 cm^2, area of battery: 14.86 cm^2) and its thickness is also thin (thickness: 1.2 mm). In addition, the weight is so small (weight of battery: 120 g) that the bulkiness can be almost negligible, and therefore, the power source for driving the device is extremely excellent in portability. It is important to reduce the amount of power consumed by the battery during operation of the device to enable long-term wireless communication while minimizing the size of the communication module.

`

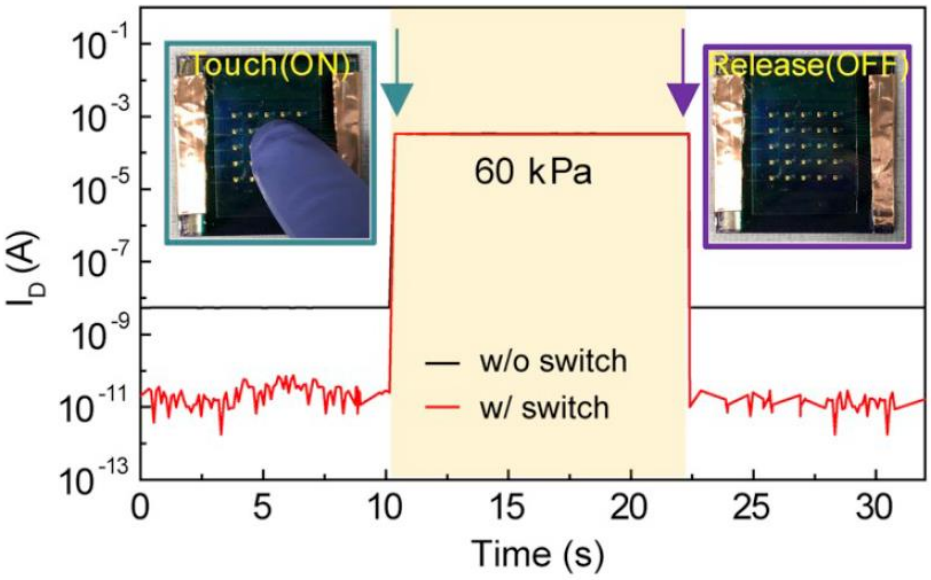

Figure 2.9. Electrical current change due to applied pressure (60 kPa).

Therefore, we have fabricated the switch to eliminate the leakage currents that transistor-based devices have when they are not turned on [20]. To prove the pressure sensor operates regardless of the presence or absence of the switch, a compression test instrument (Mark-10) was used, and the pressure was measured to be 60 kPa where the initial state of electric field at drain voltage for 5 V (V_D = 5 V) and gate voltage for 10 V (V_G = 10 V). As depicted in Figure 2.9, both the device with switch and the device without switch generate current (I_D) of 0.37 mA at the applied pressure.

`

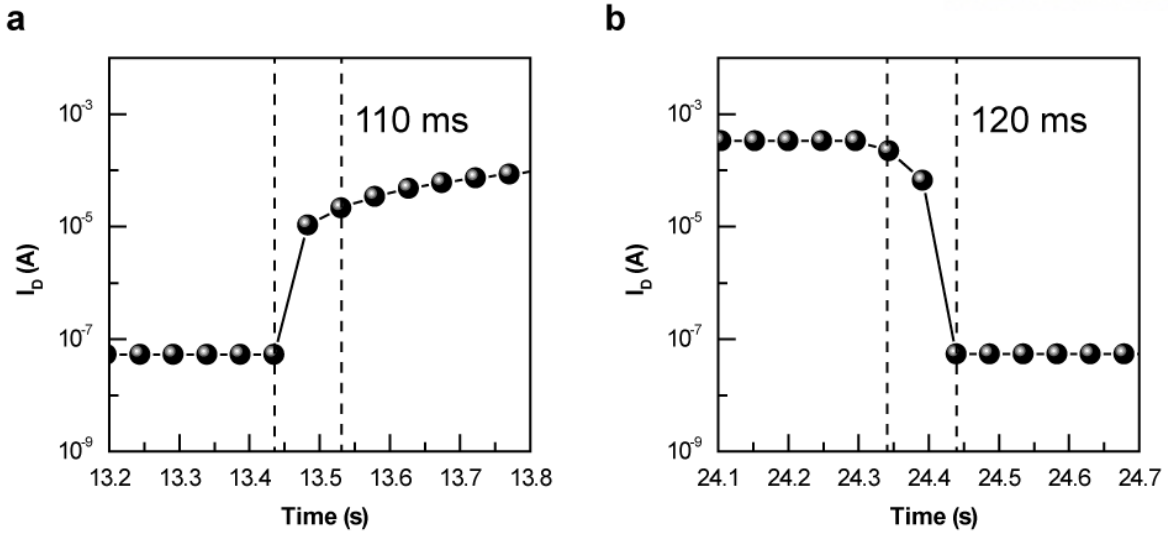

Figure 2.10. (a) The response time (~110 ms) and (b) recovery time (~120 ms) of the single pressure sensor which is measured by in real-time current plot.

In the case of a device without the switch, leakage current (IL) occurs at the level of 10^{-8} A, whereas the device with switch has the noise level of 10^{-11} A, respectively. Each of the pressure sensors showed negligible differences in response time and recovery time (response time ~ 230 ms, recovery time ~ 260 ms plot in Figure 2.10). We also proved that the resistance tunable by the contact-type switch is not large enough to affect the pressure sensor.

`

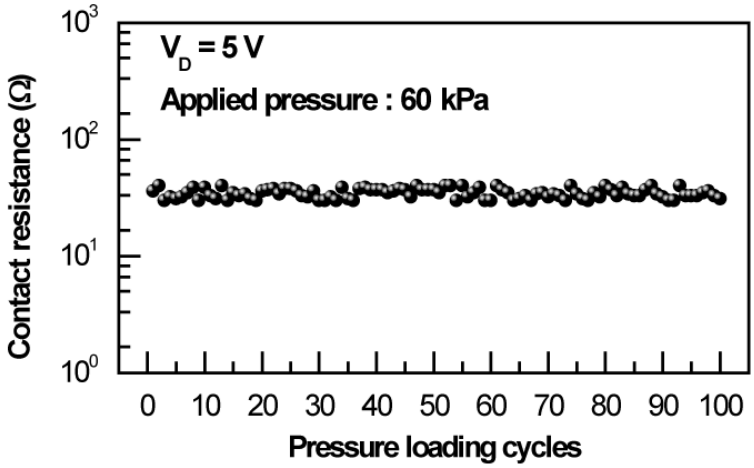

Figure 2.11. Contact resistance of the switch. The resistance is measured at VD = 5 V and constant pressure at 6 kPa with pressure application device (mark-10), the measurement was carried out 100 times under the same conditions. The contact resistance is under 35 ~ 40 Ω, which is negligible to affect the pressure sensor.

To evaluate the quality of each component before integration, Figure 2.11 show the contact pressure of the switch.

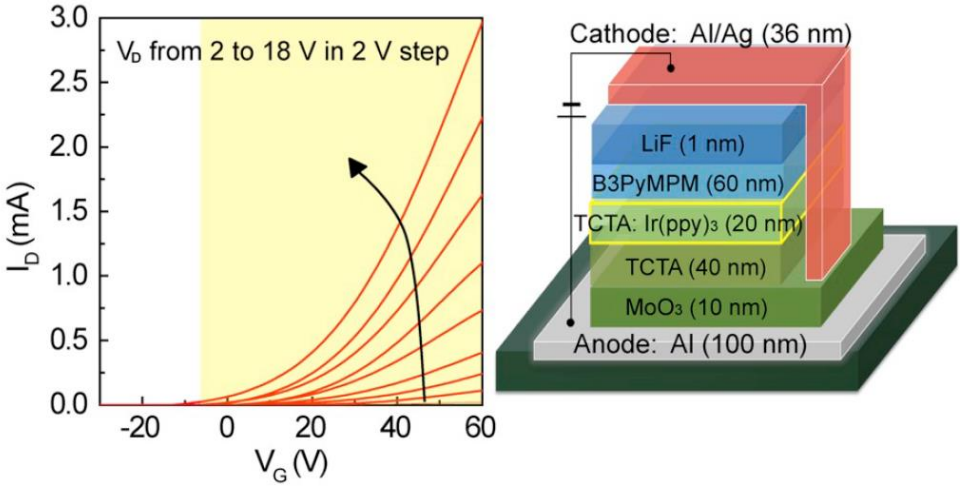

Figure 2.12. Transfer characteristics (I_D-V_G curve, V_D = 2V ~ 18 V in 2 V step) of the FET through the OLED

`

Figure 2.12 shows the transfer characteristics of the FET through the OLED when the OLED is connected in series with the pressure sensor except the switch. The OLED was formed to emit a green light through the structure as shown on the right side of the figure [21,22].

[Mechanism of pressure sensing and electrical characteristic of each components]

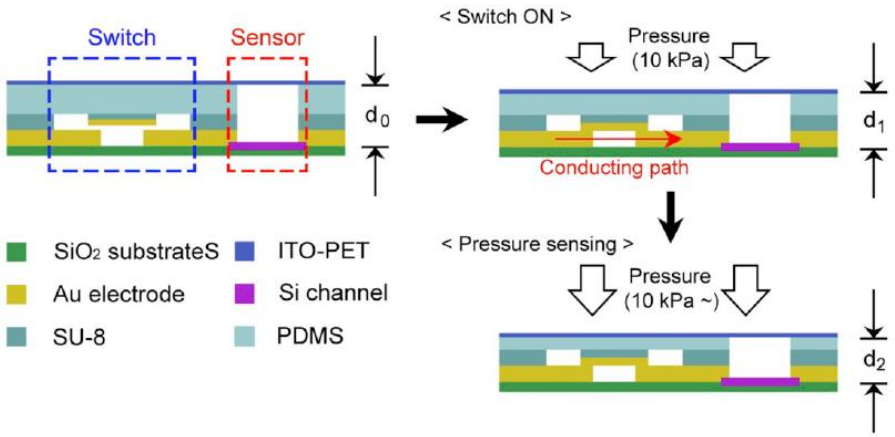

Figure 2.13. Schematic of the operating mechanisms of the switch and the pressure sensor when external pressure is applied.

Figure 2.13 shows the operating mechanisms of the switch and the pressure sensor when external pressure is applied. As shown in the first figure of the scheme (air gap thickness at d_0), in the absence of external pressure, the switch is not in contact with electrode a. When a very low pressure, i.e., 0 to 10 kPa, was applied, a conductive path of the switch was created by connecting the individual electrodes of each side of open-circuit. As higher pressures were applied, the thickness of the air gap changed depending on the amount of the pressure (air gap thickness at d_2) and PDMS condensation rate [23]. Due to the variation of the thickness of the air gap, the theoretical insulator capacitance, C_i, can be determined by Equation (1)

$$C_i = \frac{\kappa \varepsilon_0 A}{t} \quad (1)$$

where κ is a relative dielectric constant, ε_0 is the permittivity, and A and t are area and thickness of the dielectric layer, respectively. Here, κ and ε_0 are the same as those of air because the dielectric

`

layer is made of the air gap, and its values are 1.00059 (κ) and 1.0 (ε_0), so the variation of the thickness of the air gap only affects the value C_i of the pressure sensor [24–26].

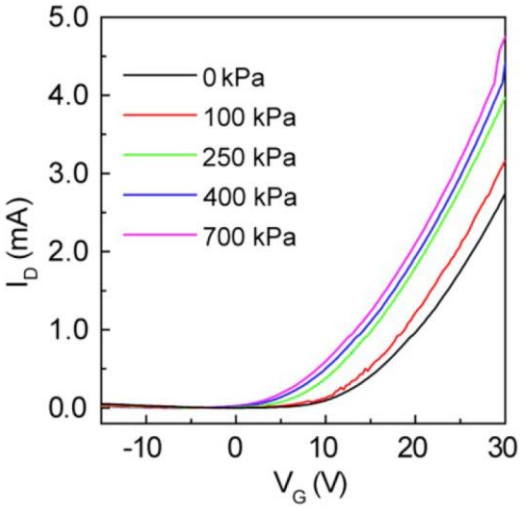

Figure 2.14. Transfer characteristics (I_D-V_G curve, V_D = 5 V) of the pressure sensor with the exception of the switch for the variation of applied pressure (0 kPa ~ 700 kPa).

Figure 2.14 shows the transfer characteristics of the pressure sensor with the exception of the switch. When the pressure is changed from 0 kPa to 700 kPa, the value of C_i increases proportionally, and the value is represented by the shift of the transfer characteristic graph. In this way, it was confirmed that the influence of the pressure at the same gate voltage (V_G) appears as the difference in the output of the drain current (I_D). Thus, with a constant V_G value, the pressure sensor clearly can represent a wide range of pressures and present a change in current.

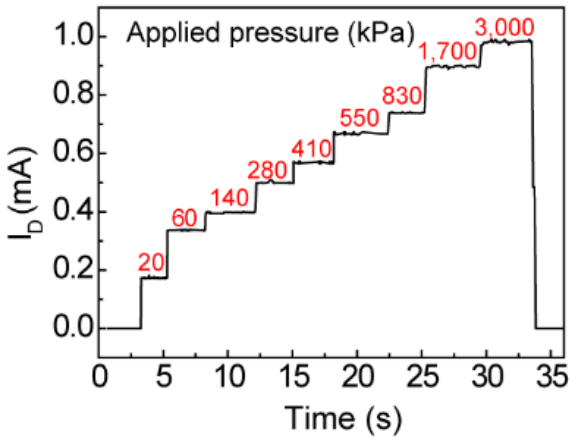

Figure 2.15. Output current change of the device with the variation of applied pressure in real time (V_D = 5 V, V_G = 10 V). Each step can be separated over a range of minimum pressures to operate the switch.

Figure 2.15 shows that the pressure of each step can be separated in real time over a range of minimum pressures to operate the switch. In order to demonstrate that a wide range of pressures can be measured accurately without additional recovery time, we measured each different pressure continuously at the V_G = 10V and V, V_D = 5 V. A commercial programmable compression test instrument was used to apply an accurate, gradually-increasing pressure to the system.

`

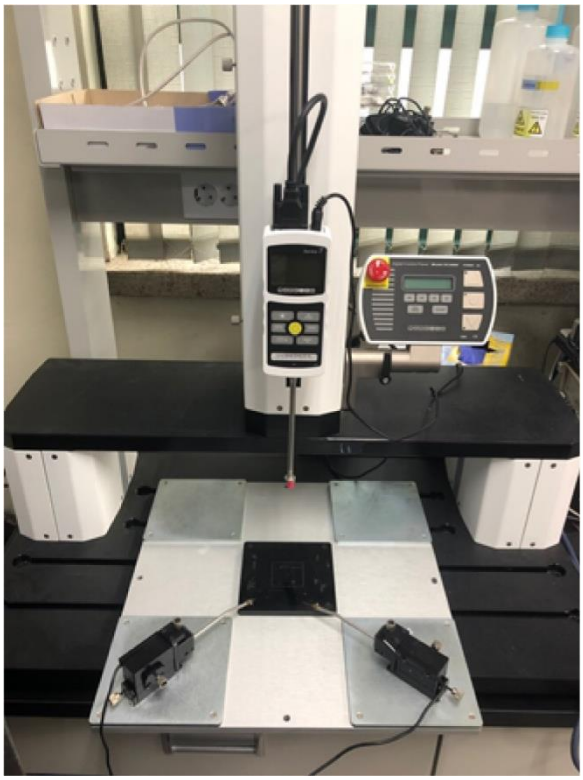

Figure 2.16. Pressure sensing apparatus. A motorized vertical test stand (Mark-10 ESM303) in combination with a force gauge (Mark-10 M7–20).

A detailed description of each step of in the application and measurement of pressure is provided in Figure 2.16 (Supporting Information). Pressures ranging from 20 kPa to 3 MPa were detected at each step in most of the areas where the pressure sensor could be used. This range of pressures could be compared to pressure of a gentle touch (the pressure when a person operates a smartphone) to the pressure of the heel. values provided by the pressure sensors allowed us visualize this exceptionally wide range of pressures.

`

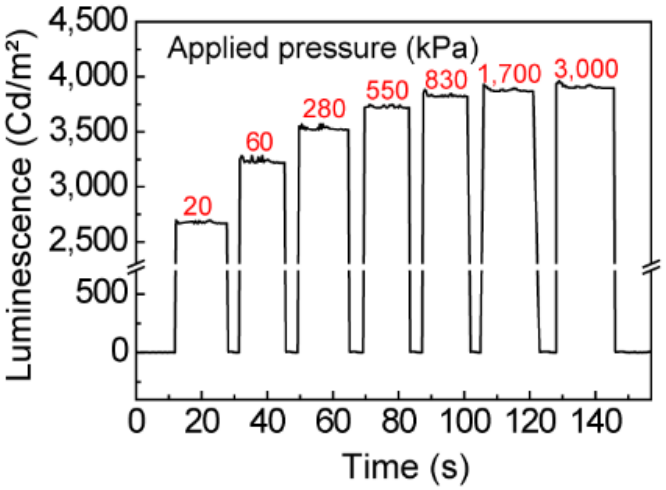

Figure 2.17. Intensity change of the light emitted from OLED connected in series with the variation of applied pressure.

Figure 2.17 shows the intensity of the light emitted from OLEDs connected in series with the pressure sensor. The intensity of the light emitted from the OLEDs was dependent on the amount of external pressure.

`

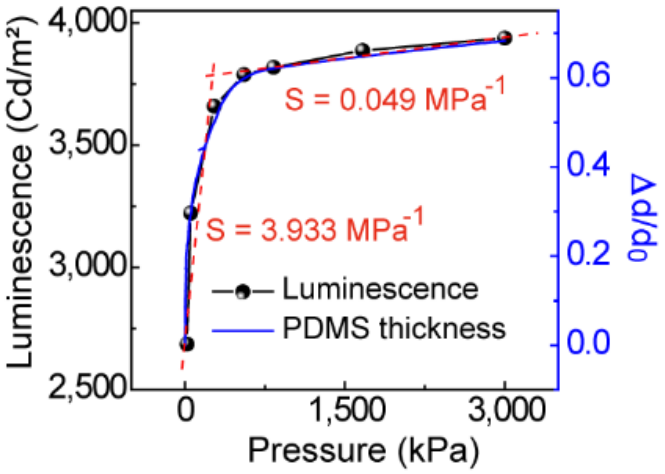

Figure 2.18. Comparison between luminescence responses of the fabricated device (pressure sensor - OLED) and true stress-strain curve from PDMS film compression test.

To measure the correct OLED brightness at each pressure step, the reactivity of the OLED lighting visualized by the external pressure was measured by extinguishing the OLED between the steps [21]. The correlation of OLED brightness over the pressure is explained in Figure 2.18. Because the change in the value of C_i is related directly to the change in the thickness of the air dielectric layer when the pressure is applied, the light change of the OLED is due to the compressibility induced at the PDMS supporting wall that creates the air dielectric layer. The graph indicates that the change in the thickness of the PDMS layer is similar to the change in the brightness of the OLED, which reflects the elastic modulus of PDMS. Thus, the change in the thickness of the PDMS layer relates directly to the brightness of the OLED. Thus, the measurement principle of the pressure sensor and its results can be demonstrated clearly.

`

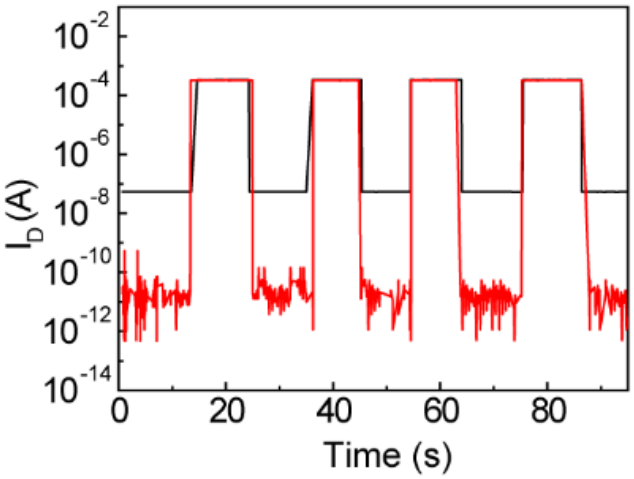

Figure 2.19. Comparison of response value for pressure sensor with presence or absence of switch under the same applied pressure of 60 kPa in real time.

In order to determine the effect of the switch on the repetitive operation of the device, pressure sensors with and without switches were compared by applying the same pressure [14,27]. Figure 2.19 shows that the response value of each sensor was measured with the pressure of 60 kPa. The pressure sensor with switch shows that the base current of the noise level is 3×10^{-12} A, but the switchless pressure sensor shows a current leakage of about ~ 2×10^{-8} A. The results shows that the current response at a pressure of 60 kPa was 350 (±10) μA irrespective of whether or not there was a switch. Therefore, the results indicated that the existence of the switch does not affect the sensitivity of the pressure sensor, resulting in advantages for a wireless communication system.

`

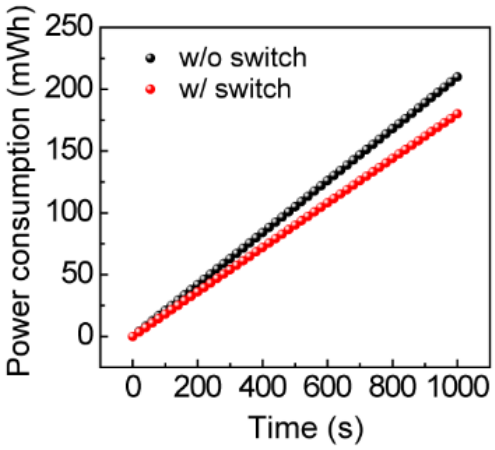

Figure 2.20. Comparison of power consumption with presence or absence of switch when the repetitive pressure sensor operation is performed.

Figure 2.20 shows how the presence of the switch can benefit from the power consumption when the repetitive pressure sensor operation is performed. It is apparent that the power consumption of ~5 mWh per minute can be prevented by the switch when the same conditions shown in Figure 2.20 exist. Considering the size of the entire device and the battery [28], it is an effective method for preventing unnecessary power consumption. Although the method of comparison can be different, when the leakage current is blocked at each pixel and goes to the entire device, the effect of the switch becomes larger over time, which is a significant advantage for wireless communication and the miniaturization of the device.

`

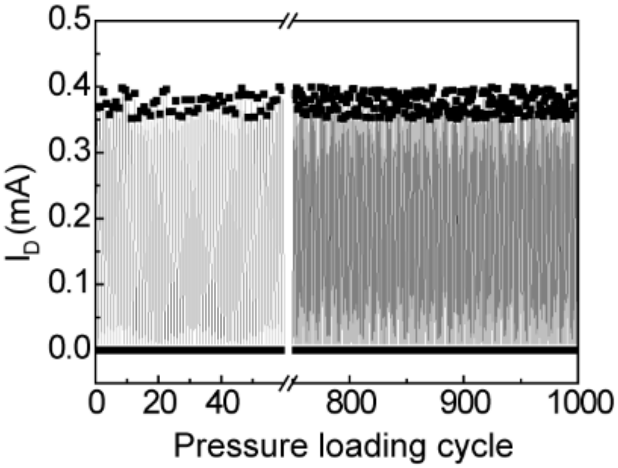

Figure 2.21. Cyclic test of the pressure sensor under the pressure of 60 kPa.

Figure 2.21 shows the results of a cyclic pressure test that was conducted to prove the reliability and durability of the pressure sensor. In this test, a pressure of 60 kPa was applied and repeated 1,000 times. During this cyclic test, the average value of the normalized change of I_D at the pressure of 60 kPa was calculated as 350.23 μA with a standard deviation of 0.00264 at V_D = 5 V and V_G = 10 V.

`

2.2.3. Conclusion

The resulting device that interacts with humans by integrating heterogeneous components together such as sensors, luminaire, and communication modules presents the possibility of transmitting physical stimulation (pressure) to other platforms wirelessly. The FET type pressure sensor consisting of the Si channel uses the air as a dielectric layer to read a wide range of pressure as well as the structural characteristics of the FET as the role of a switch, and it can reduce the standby power the driving power. The switch operated by pressure can simply be turned on and off for a very weak stimulation (touch) without a separate electrical device so that it provides the battery with enhanced its quality.

`

3. Integrated wireless system with pressure sensor

3.1. Research background

[Wireless communication system with pressure sensor]

Through the construction of a system capable of these wireless communications, we expect the expansion of the field of the sensor by enabling free conversion of the results of the sensor to digital data [29-34]. Accordingly, results have been very promising so far to advance in the field of soft electronics and biomedical science through the technologies that enable wireless communication system between electronic sensors and mobile devices, therefore miniaturization and low driving power of devices.

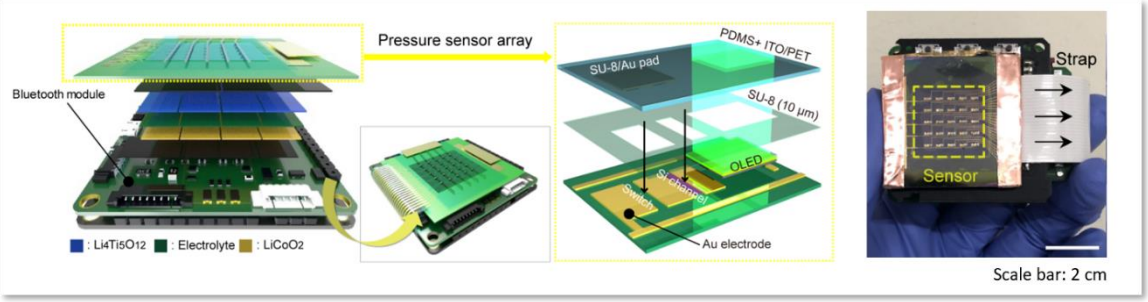

- **Custom-made Bluetooth module is integrated with the sensor to transmit current information to the smartphone wirelessly**

Figure 3.1. Integrated system with pressure sensor and Bluetooth module.

`

3.2. Experiments

3.2.1. Experimental methods

[Integration of sensor, battery, and communication module]

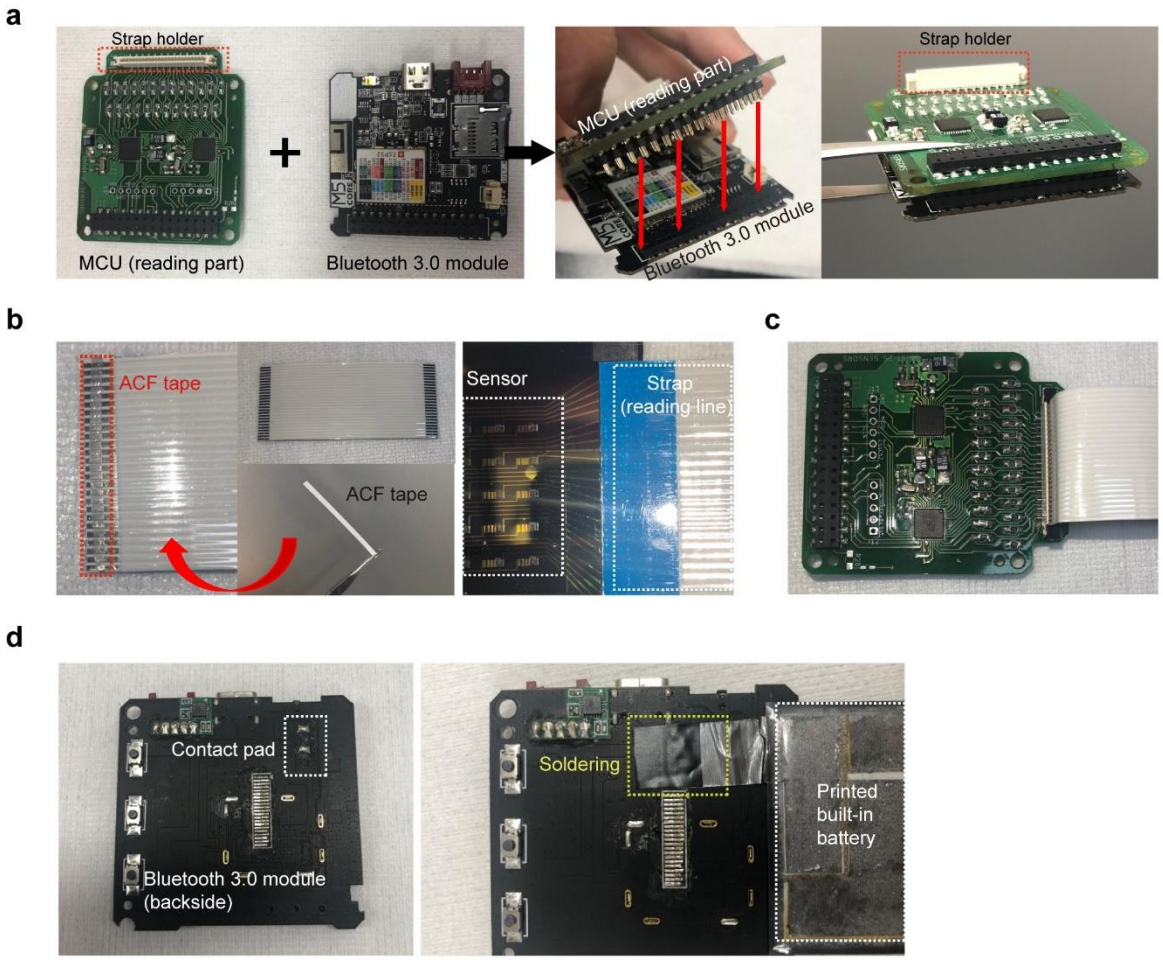

Figure 3.2. Actual photographs of communication module. (a) Structure of connection between MCU and Bluetooth module. Two boards are connected with board-to-board connector (elevated pin header). (b) Connection between sensor electrode pad and flat, flexible cable (FFC) by ACF bonding. (c) Connection between MCU and FFC with strap holder. (d) Connection between contact pad of Bluetooth module and interconnect of printed built-in battery by soldering technique.

`

A strap-type, flat, flexible cable (FFC) was fixed to the electrode pad pattern from the drain of the sensor using anisotropic conducting film (ACF) bonding. When ACF bonding, tape type ACF was fixed between the substrate pad and the strap using native adhesive force of the ACF itself. Then, heat of 90° was applied by hot plate while 3 MPa of pressure was applied for 1 second. The other side of the strap is connected to the strap holder of micro controller unit (MCU) board. The MCU board and Bluetooth board are connected with board-to-board connector (elevated pin header). A thin strap-type interconnect of the printed built-in battery is connected together with contact pad of Bluetooth module by soldering technique. After the interconnect and contact pad are connected together, a substrate of sensor is combined with the module by adhesive resin.

`

3.2.2. Results and discussion

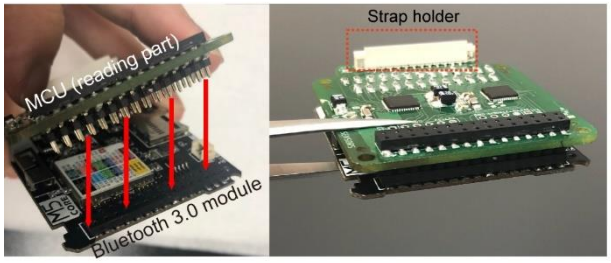

Figure 3.3. Actual photographs of integrated module with the part of MCU and Bluetooth.

The integration of the pressure sensor and the battery minimizes the size of the entire device and maximizes the efficiency of the battery by operating the switch. Therefore, the device has high portability due to its small size and light weight. It can be used for a long time with high efficiency of the battery. In order to utilize these features and make it more useful, we have implemented a device that can continuously communicate with a smartphone while compactly adding a custom-made module (Bluetooth 4.0; width: 5.2 cm, length: 5.25 cm, thickness: 1.2 cm) that enables wireless communication.

The module modifies the signal from a sensor that sends an electrical signal in response to pressure to a form of data suitable for Bluetooth communication and transmits the data to the smartphone to quantify the measured pressure value.

`

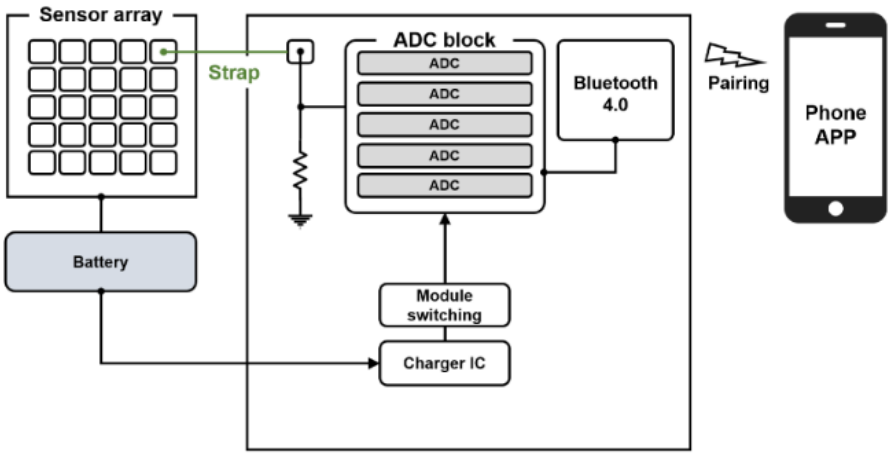

Figure 3.4. Corresponding electrical circuitry for active-matrix sensor array which allows selective readout of electrical response and wireless transmission to the smartphone.

As shown in Figure 3.4, there are five analog-to-digital converters (ADC) in the module. Using five ADCs, the module can simultaneously measure and convert electrical signals from the entire sensor, avoiding any temporal delays in the process. A strap type flat flexible cable (FFC) with a 2.53 mm pitch length was fixed to the pressure sensor contact pad by soldering to transmit the electrical signal from the sensor to the module, and a dedicated connector was attached to the PCB board on the module side.

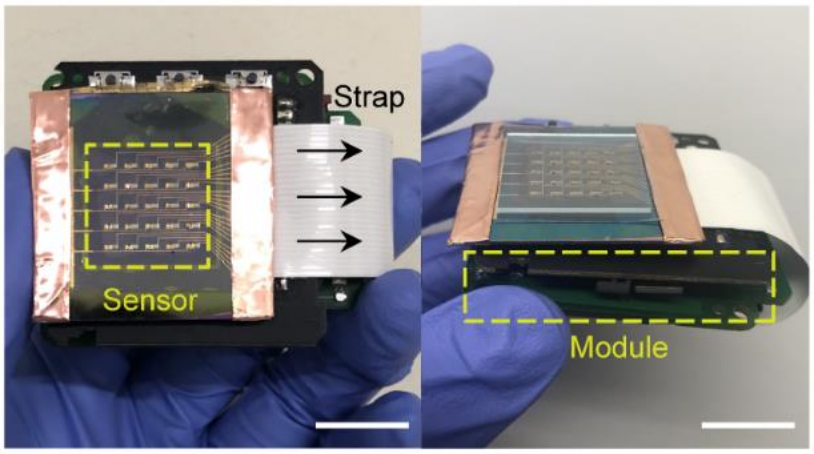

Figure 3.5. Photographs of integrated device which is composed of pressure sensor, built-in battery, and Bluetooth module. Scale bar, 2 cm.

The FFC is bent sufficiently to connect the sensor substrate and the module, which are composed of the bilayer, leading the volume of the device to be small (Figure 3.5).

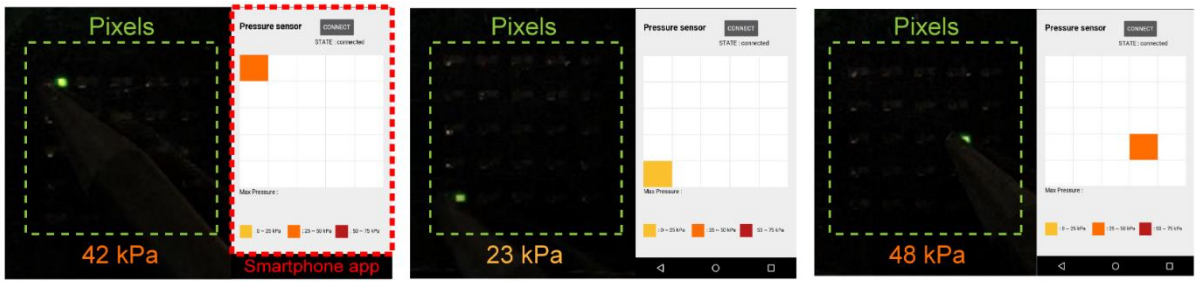

Figure 3.6. Photographs of single sensor pixel that emit light in response to applied pressure and captured images of a smartphone which received pressure information by wireless communication.

`

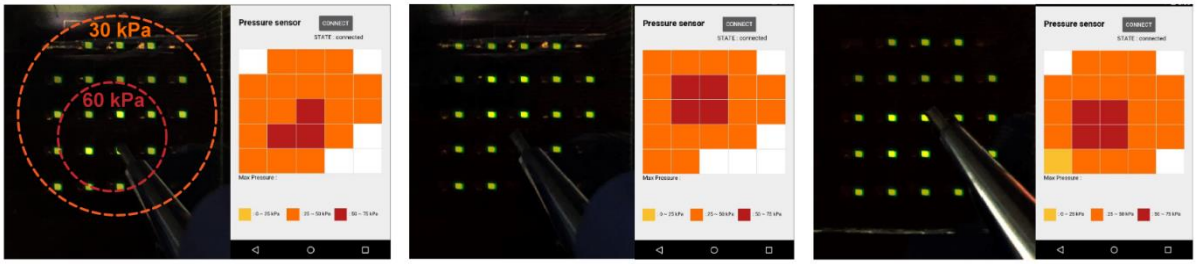

Figure 3.7. Photographs of sensor array that emit light in response to applied pressure and captured images of a smartphone which received pressure information by wireless communication.

Figure 3.6, Figure 3.7 show characteristics of OLED emission due to the pressure imposed on sensors and corresponding smartphone communication screen. Each was demonstrated using a pen to apply pressure to one sensor (one pixel) and to a large area of PET (thickness: 2 mm) simultaneously.

It can be seen that the brightness of the OLED is changed by reflecting the change of the current transmitted depending on the magnitude of the pressure. In addition, the numerical value of the current change value depending on the pressure force imposed at the sensors is displayed on the screen of the smartphone through Bluetooth wireless communication and divided into different colors on the screen.

`

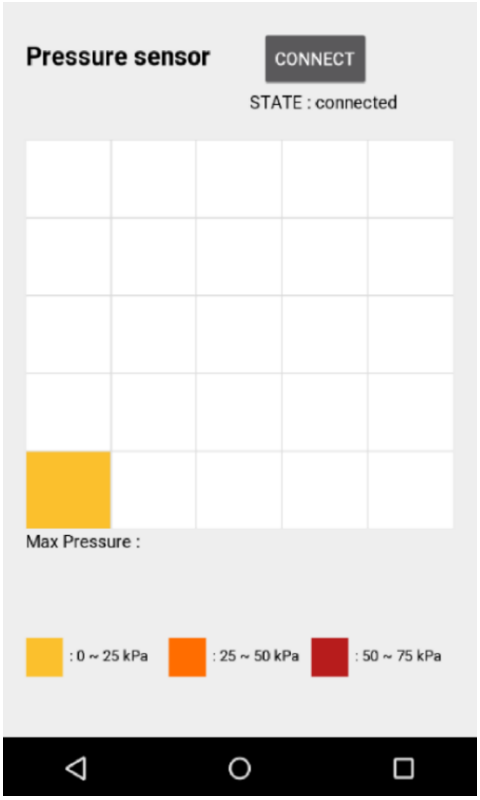

Figure 3.8. Displayed pressure force imposed at the sensors on the screen of the smartphone through Bluetooth wireless communication

As depicted in Figure 3.8, the pressure range is in range of 0 ~ 25 kPa (yellow), 25 ~ 50 kPa (orange) and 50 ~ 75 kPa (red). When the pressure is applied to a wide area of PET, the switch does not operate under a pressure of 10 kPa or less. And, the light emitted from the OLED does not occur at a very low range of the pressure. In addition, it can be seen that the concentration of the pressure is divided by the point where the pen is pressing with higher pressure.

This shows that the brightness of the OLED coincides with that of the smartphone screen. Therefore, we implemented visualization in two ways depending on the magnitude of the pressure, OLED emission and representation on the smartphone screen.

`

3.2.3. Conclusion

In the minimum size matter, which is one of the most important factors for integrating the wireless communication device, the novel built-in type battery was integrated with the sensor. We demonstrated the entire wireless communication system which is wirelessly communicated with the smartphone in real time. Therefore, it contributes to interactive display that operates in response to human behavior, various robotics fields using wireless communication through immediate visualization of pressure. The resulting device that interacts with humans by integrating heterogeneous components together such as sensors, luminaire, and communication modules presents the possibility of transmitting physical stimulation (pressure) to other platforms wirelessly.

`

4. Conclusion

The resulting device that interacts with humans by integrating heterogeneous components together such as sensors, luminaire, and communication modules presents the possibility of transmitting physical stimulation (pressure) to other platforms wirelessly [11]. The FET type pressure sensor consisting of the Si channel uses the air as a dielectric layer to read a wide range of pressure as well as the structural characteristics of the FET as the role of a switch, and it can reduce the standby power the driving power [6-8].

The switch operated by pressure can simply be turned on and off for a very weak stimulation (touch) without a separate electrical device so that it provides the battery with enhanced life for the wireless device. In the minimum size matter, which is one of the most important factors for integrating the wireless communication device, the novel built-in type battery was integrated with the sensor [14, 17, 23].

We demonstrated the entire wireless communication system which is wirelessly communicated with the smartphone in real time. We showed the system of displaying the pressure value measured in real time on the screen of the mobile devices which is expected to advance in the fields of soft electronics and biomedical science. In order to improve the portability of the pressure sensor and improve the applicability, the process was performed on a new substrate through hybridization of the rigid part and the soft part so as to allow conformal contact to curved objects as well as rigid glass-based substrates. Through the process in the rigid part, the protection of the main components is ensured and flexibility and stretchability are ensured by the deformation of the soft part. Because it is applicable to various biocomponents such as organ organs, insects or surface of plants, the pressure sensor using this structure has wide expandability in biomedical field [36-41].

Therefore, it contributes to interactive display that operates in response to human behavior, various robotics fields using wireless communication through immediate visualization of pressure. Also, our development of the human-interactive display is promising in future advance in the fields of soft electronics and biomedical science with the use of the integration and miniaturization technology.

`

5. References

[1] Y. Khan, A.E. Ostfeld, C.M. Lochner, A. Pierre, A.C. Arias, Monitoring of Vital Signs with Flexible and Wearable Medical Devices, Advanced Materials. 28 (2016) 4373–4395. doi:10.1002/adma.201504366.

[2] S. Wang, L. Lin, Z.L. Wang, Triboelectric nanogenerators as self-powered active sensors, Nano Energy. 11 (2015) 436–462. doi:10.1016/j.nanoen.2014.10.034.

[3] T. Yokota, P. Zalar, M. Kaltenbrunner, H. Jinno, N. Matsuhisa, H. Kitanosako, Y. Tachibana, W. Yukita, M. Koizumi, T. Someya, Ultraflexible organic photonic skin, Sci Adv. 2 (2016) e1501856. doi:10.1126/sciadv.1501856.

[4] C. Wang, D. Hwang, Z. Yu, K. Takei, J. Park, T. Chen, B. Ma, A. Javey, User-interactive electronic skin for instantaneous pressure visualization, Nature Materials. 12 (2013) 899.

[5] M. Peng, Z. Li, C. Liu, Q. Zheng, X. Shi, M. Song, Y. Zhang, S. Du, J. Zhai, Z.L. Wang, High-Resolution Dynamic Pressure Sensor Array Based on Piezo-phototronic Effect Tuned Photoluminescence Imaging, ACS Nano. 9 (2015) 3143–3150. doi:10.1021/acsnano.5b00072.

[6] S. Jung, J.H. Kim, J. Kim, S. Choi, J. Lee, I. Park, T. Hyeon, D.-H. Kim, Reverse-Micelle-Induced Porous Pressure-Sensitive Rubber for Wearable Human–Machine Interfaces, Advanced Materials. 26 (2014) 4825–4830. doi:10.1002/adma.201401364.

[7] S. Ji, J. Jang, E. Cho, S.-H. Kim, E.-S. Kang, J. Kim, H.-K. Kim, H. Kong, S.-K. Kim, J.-Y. Kim, J.-U. Park, High Dielectric Performances of Flexible and Transparent Cellulose Hybrid Films Controlled by Multidimensional Metal Nanostructures, Advanced Materials. 29 (2017) 1700538. doi:10.1002/adma.201700538.

[8] S.C.B. Mannsfeld, B.C.-K. Tee, R.M. Stoltenberg, C.V.H.-H. Chen, S. Barman, B.V.O. Muir, A.N. Sokolov, C. Reese, Z. Bao, Highly sensitive flexible pressure sensors with microstructured rubber dielectric layers, Nature Materials. 9 (2010) 859.

[9] T. Someya, T. Sekitani, S. Iba, Y. Kato, H. Kawaguchi, T. Sakurai, A large-area, flexible pressure sensor matrix with organic field-effect transistors for artificial skin applications, Proc Natl Acad Sci U S A. 101 (2004) 9966. doi:10.1073/pnas.0401918101.

[10] S.-H. Shin, S. Ji, S. Choi, K.-H. Pyo, B. Wan An, J. Park, J. Kim, J.-Y. Kim, K.-S. Lee, S.-Y. Kwon, J. Heo, B.-G. Park, J.-U. Park, Integrated arrays of air-dielectric graphene transistors as transparent active-matrix pressure sensors for wide pressure ranges, Nature Communications. 8 (2017) 14950.

[11] H. Lee, S. Chang, E. Yoon, A Flexible Polymer Tactile Sensor: Fabrication and Modular Expandability for Large Area Deployment, Journal of Microelectromechanical Systems. 15 (2006) 1681–1686. doi:10.1109/JMEMS.2006.886021.

`

[12] H.-D. Um, K.-H. Choi, I. Hwang, S.-H. Kim, K. Seo, S.-Y. Lee, Monolithically integrated, photo-rechargeable portable power sources based on miniaturized Si solar cells and printed solid-state lithium-ion batteries, Energy & Environmental Science. 10 (2017) 931–940. doi:10.1039/C6EE03266D.

[13] S.-H. Kim, K.-H. Choi, S.-J. Cho, J. Yoo, S.-S. Lee, S.-Y. Lee, Flexible/shape-versatile, bipolar all-solid-state lithium-ion batteries prepared by multistage printing, Energy Environ. Sci. 11 (2018) 321–330. doi:10.1039/C7EE01630A.

[14] Q. Sun, D.H. Kim, S.S. Park, N.Y. Lee, Y. Zhang, J.H. Lee, K. Cho, J.H. Cho, Transparent, Low-Power Pressure Sensor Matrix Based on Coplanar-Gate Graphene Transistors, Advanced Materials. 26 (2014) 4735–4740. doi:10.1002/adma.201400918.

[15] S.R. Forrest, The path to ubiquitous and low-cost organic electronic appliances on plastic, Nature. 428 (2004) 911.

[16] J. Park, J. Kim, K. Kim, S.-Y. Kim, W. Hyung Cheong, K. Park, J. Hyeb Song, G. Namgoong, J. Joon Kim, J. Heo, F. Bien, J.-U. Park, Wearable, wireless gas sensors using highly stretchable and transparent structures of nanowires and graphene, Nanoscale. 8 (2016) 10591–10597. doi:10.1039/C6NR01468B.

[17] S. Lim, D. Son, J. Kim, Y.B. Lee, J.-K. Song, S. Choi, D.J. Lee, J.H. Kim, M. Lee, T. Hyeon, D.-H. Kim, Transparent and Stretchable Interactive Human Machine Interface Based on Patterned Graphene Heterostructures, Advanced Functional Materials. 25 (2015) 375–383. doi:10.1002/adfm.201402987.

[18] J. Park, J. Kim, S.-Y. Kim, W.H. Cheong, J. Jang, Y.-G. Park, K. Na, Y.-T. Kim, J.H. Heo, C.Y. Lee, J.H. Lee, F. Bien, J.-U. Park, Soft, smart contact lenses with integrations of wireless circuits, glucose sensors, and displays, Sci Adv. 4 (2018) eaap9841. doi:10.1126/sciadv.aap9841.

[19] C.M. Boutry, L. Beker, Y. Kaizawa, C. Vassos, H. Tran, A.C. Hinckley, R. Pfattner, S. Niu, J. Li, J. Claverie, Z. Wang, J. Chang, P.M. Fox, Z. Bao, Biodegradable and flexible arterial-pulse sensor for the wireless monitoring of blood flow, Nature Biomedical Engineering. 3 (2019) 47. doi:10.1038/s41551-018-0336-5.

[20] Y. Liu, J. Liu, S. Chen, T. Lei, Y. Kim, S. Niu, H. Wang, X. Wang, A.M. Foudeh, J.B.-H. Tok, Z. Bao, Soft and elastic hydrogel-based microelectronics for localized low-voltage neuromodulation, Nature Biomedical Engineering. 3 (2019) 58. doi:10.1038/s41551-018-0335-6.

[21] H. Becker, S.E. Burns, R.H. Friend, Effect of metal films on the photoluminescence and electroluminescence of conjugated polymers, Phys. Rev. B. 56 (1997) 1893–1905. doi:10.1103/PhysRevB.56.1893.

[22] M. Ikai, S. Tokito, Y. Sakamoto, T. Suzuki, Y. Taga, Highly efficient phosphorescence from organic light-emitting devices with an exciton-block layer, Applied Physics Letters. 79 (2001) 156–158.

[23] I.D. Johnston, D.K. McCluskey, C.K.L. Tan, M.C. Tracey, Mechanical characterization of bulk Sylgard 184 for microfluidics and microengineering, J. Micromech. Microeng. 24 (2014) 035017. doi:10.1088/0960-1317/24/3/035017.

[24] R.H. Friend, R.W. Gymer, A.B. Holmes, J.H. Burroughes, R.N. Marks, C. Taliani, D.D.C. Bradley, D.A.D. Santos, J.L. Brédas, M. Lögdlund, W.R. Salaneck, Electroluminescence in conjugated polymers, Nature. 397 (1999) 121.

[25] A.C. Arias, J.D. MacKenzie, I. McCulloch, J. Rivnay, A. Salleo, Materials and Applications for Large Area Electronics: Solution-Based Approaches, Chem. Rev. 110 (2010) 3–24. doi:10.1021/cr900150b.

[26] S.-H. Kim, K.-H. Choi, S.-J. Cho, S. Choi, S. Park, S.-Y. Lee, Printable Solid-State Lithium-Ion Batteries: A New Route toward Shape-Conformable Power Sources with Aesthetic Versatility for Flexible Electronics, Nano Lett. 15 (2015) 5168–5177. doi:10.1021/acs.nanolett.5b01394.

[27] E.-H. Kil, K.-H. Choi, H.-J. Ha, S. Xu, J.A. Rogers, M.R. Kim, Y.-G. Lee, K.M. Kim, K.Y. Cho, S.-Y. Lee, Imprintable, Bendable, and Shape-Conformable Polymer Electrolytes for Versatile-Shaped Lithium-Ion Batteries, Advanced Materials. 25 (2013) 1395–1400. doi:10.1002/adma.201204182.

[28] S.-H. Kim, K.-H. Choi, S.-J. Cho, J.-S. Park, K. Young Cho, C. Kee Lee, S. Bong Lee, J. Kie Shim, S.-Y. Lee, A shape-deformable and thermally stable solid-state electrolyte based on a plastic crystal composite polymer electrolyte for flexible/safer lithium-ion batteries, Journal of Materials Chemistry A. 2 (2014) 10854–10861. doi:10.1039/C4TA00494A.

[29] T. Tsuchiya, T. Kobayashi, S. Nakajima, Hot-carrier-injected oxide region and hot-electron trapping as the main cause in Si nMOSFET degradation, IEEE Transactions on Electron Devices. 34 (1987) 386–391. doi:10.1109/T-ED.1987.22934.

[30] H.S.P. Wong, K.K. Chan, Y. Taur, Self-aligned (top and bottom) double-gate MOSFET with a 25 nm thick silicon channel, in: International Electron Devices Meeting. IEDM Technical Digest, 1997: pp. 427–430. doi:10.1109/IEDM.1997.650416.

[31] L. Boodhoo, L. Crudgington, H.M.H. Chong, Y. Tsuchiya, Z. Moktadir, T. Hasegawa, H. Mizuta, Fabrication and characterisation of suspended narrow silicon nanowire channels for low-power nano-electro-mechanical (NEM) switch applications, Microelectronic Engineering. 145 (2015) 66–70. doi:10.1016/j.mee.2015.02.047.

[32] M. Kang, J. Kim, B. Jang, Y. Chae, J.-H. Kim, J.-H. Ahn, Graphene-Based Three-Dimensional Capacitive Touch Sensor for Wearable Electronics, ACS Nano. 11 (2017) 7950–7957. doi:10.1021/acsnano.7b02474.

[33] J.-K. Song, D. Son, J. Kim, Y.J. Yoo, G.J. Lee, L. Wang, M.K. Choi, J. Yang, M. Lee, K. Do, J.H. Koo, N. Lu, J.H. Kim, T. Hyeon, Y.M. Song, D.-H. Kim, Wearable Force Touch Sensor Array Using a Flexible and Transparent Electrode, Adv. Funct. Mater. 27 (2017) n/a-n/a. doi:10.1002/adfm.201605286.

[34] S.A. Bus, J.S. Ulbrecht, P.R. Cavanagh, Pressure relief and load redistribution by custom-made insoles in diabetic patients with neuropathy and foot deformity, Clinical Biomechanics. 19 (2004) 629–638. doi:10.1016/j.clinbiomech.2004.02.010.

[35] Y. Gao, H. Ota, E.W. Schaler, K. Chen, A. Zhao, W. Gao, H.M. Fahad, Y. Leng, A. Zheng, F. Xiong, C. Zhang, L.-C. Tai, P. Zhao, R.S. Fearing, A. Javey, Wearable Microfluidic Diaphragm Pressure Sensor for Health and Tactile Touch Monitoring, Adv. Mater. 29 (2017) n/a-n/a. doi:10.1002/adma.201701985.

[36] W. Honda, S. Harada, T. Arie, S. Akita, K. Takei, Wearable, Human-Interactive, Health-Monitoring, Wireless Devices Fabricated by Macroscale Printing Techniques, Adv. Funct. Mater. 24 (2014) 3299–3304. doi:10.1002/adfm.201303874.

[37] L.Y. Chen, B.C.-K. Tee, A.L. Chortos, G. Schwartz, V. Tse, D.J. Lipomi, H.-S.P. Wong, M.V. McConnell, Z. Bao, Continuous wireless pressure monitoring and mapping with ultra-small passive sensors for health monitoring and critical care, Nature Communications. 5 (2014) 5028. doi:10.1038/ncomms6028.

[38] B.W. An, J.H. Shin, S.-Y. Kim, J. Kim, S. Ji, J. Park, Y. Lee, J. Jang, Y.-G. Park, E. Cho, S. Jo, J.-U. Park, Smart Sensor Systems for Wearable Electronic Devices, Polymers. 9 (2017) 303. doi:10.3390/polym9080303.

[39] S. Lee, A. Reuveny, J. Reeder, S. Lee, H. Jin, Q. Liu, T. Yokota, T. Sekitani, T. Isoyama, Y. Abe, Z. Suo, T. Someya, A transparent bending-insensitive pressure sensor, Nat Nano. 11 (2016) 472–478. doi:10.1038/nnano.2015.324.

[40] S. Park, H. Kim, M. Vosgueritchian, S. Cheon, H. Kim, J.H. Koo, T.R. Kim, S. Lee, G. Schwartz, H. Chang, Z. Bao, Stretchable Energy-Harvesting Tactile Electronic Skin Capable of Differentiating Multiple Mechanical Stimuli Modes, Adv. Mater. 26 (2014) 7324–7332. doi:10.1002/adma.201402574.

[41] S.C.B. Mannsfeld, B.C.-K. Tee, R.M. Stoltenberg, C.V.H.-H. Chen, S. Barman, B.V.O. Muir, A.N. Sokolov, C. Reese, Z. Bao, Highly sensitive flexible pressure sensors with microstructured rubber dielectric layers, Nat Mater. 9 (2010) 859–864. doi:10.1038/nmat2834.

`

6. Acknowledgements

This work was supported by my advisor, Prof. Jang-Ung Park, and my lab members in WEL lab. Most of all, I would like to thank my advisor, Prof. Jang-Ung Park, for his supervision and encouragements during my master's course. He gave me an answer to the question of whether I could do research that would make more valuable and convenient people from existing studies, and he gave me specific directions on what to do next. Under his guidance, I learned effectively how to start a study, how to approach it, how to finish it, and how to write a paper. Moreover, his power of execution has always motivated and inspired me to grow as active researcher in this field.

I also thank Prof. Myoung Hoon Song and Sang-Young Lee as committee members for my thesis evaluation. They deserve my deepest appreciation because of their devoted help and support including professional discussions and collaboration opportunities.

In addition, I would also like to thank both the present members (Dr. Hyeon Seok An, Dr. Joohee Kim, Dr. Jihun Park, Dr. Sangyoon Ji, Jiuk Jang, Young-Geun Park, Jae Chul Hwang, Byungkook Oh, Minjae Ku, Gon Guk Kim, Hyobeom Kim, Eun Kyung Cha, Sang Il Lee, Sang Beom Bak, Inho Park and Yohan Cho) and past members (Dr. Kukjoo Kim, Dr. Hungu Kang, Dr. Jihyun Paek, Prof. Jung Hwal Shin, Dr. Byung Gwan Hyun, Dr. So-Yun Kim, Mijung Kim, Sung-Ho Shin, Eunjin Cho, Subin Jo, and Seoyeong Ju) of our lab for a long period of time together with me for about 4 years. I learned a lot. Thank you.

Finally, I would like to thank all of my family for their unlimited support during the master's course. Thank you for your help over the long time.

I give praise to myself for long years of hard work.